Available online at www.sciencedirect.com
SCIENCE DIRECT®
Journal of Sound and Vibration 277 (2004) 73–100
JOURNAL OF SOUND AND VIBRATION
www.elsevier.com/locate/jsvi

# Continuous wavelet transform for modal identification using free decay response

Thien-Phu Le*, Pierre Argoul

*Laboratoire Analyse des Matériaux et Identification, LAMI (ENPC/LCPC, Institut Navier) ENPC, 6-8, Avenue Blaise Pascal, 77455 Champs sur Marne, Marne-la-Vallee cedex, France*

Received 13 January 2003; accepted 20 August 2003

**Abstract**

This paper deals with the use of the continuous wavelet transform for system identification purposes. The wavelet analysis of the free responses of a linear mechanical system allows the estimation of its natural frequencies, viscous damping ratios and mode shapes, using either the modulus or the phase of the wavelet transform. A complete procedure for modal identification from free responses based on the continuous wavelet transform is presented. Two difficulties during the implementation of this technique are highlighted: the edge effect and the choice of the time–frequency localization of the wavelet transform. Some upper and lower bounds for the mother wavelet's parameters are given in order to improve the numerical computation. Three complex-valued mother wavelets are studied and the full procedure is applied to a damped discrete system. The correct choice of the mother wavelet's parameters leads to an accurate identification of the modal parameters.


## 1. Introduction

The number of algorithms that have been developed over the past 30 years, to estimate modal parameters from measured frequency or impulse response function data is considerable. The modal analysis identification method presented in this paper, is based upon the use of continuous wavelet transform (CWT). The measured signals are free-decay responses of mechanical structures which are then processed with a time–frequency transform. Referring to the concept of characteristic space introduced by Allemang and Brown [1] to represent measurement data, the temporal axis of this method is neither time nor frequency but rather is substituted by a

*Corresponding author. Tel.: +33-64-153736; fax: +33-64-153741.
*E-mail address:* le@lami.enpc.fr (T.-P. Le).

0022-460X/$ - see front matter 
doi:10.1016/j.jsv.2003.08.049

time–frequency plane. The time–frequency representation allows the time variation of the instantaneous amplitude and phase of each component within the measured signals to be determined. Moreover, if the general classification for identification methods given in Ref. [2] is used, the identification method is indirect in the sense that it estimates the modal parameters (natural frequencies, damping ratios, modal constants and their phases); it can be applied to multi-degree-of-freedom (m.d.o.f) systems and is a single-input–multi-output (SIMO) method. Regarding the class of SIMO and m.d.o.f, the most widely known are, in the time domain, the least-squares complex exponential (LSCE) [3] and the Ibrahim time domain (ITD) [4]; in the frequency domain, the global rational fraction polynomial [5] (GRFP). The LSCE and the ITD approaches allow the modal parameters to be extracted from damped complex exponential response information. The ITD method uses free decay responses instead of impulse response functions used in the LSCE method. The GRFP is an extension of the very popular and widely used rational fraction polynomial (RFP) method [6] to analyse globally a set of frequency response functions using one single input reference.

In the proposed technique, the processed signals can be considered, under certain conditions such as the assumption of weak damping, as a sum of components consisting of asymptotic frequency modulated signals. The wavelet analysis of such signals highlights the maximum amount of information within the data: it has a tendency to concentrate near a series of curves called ridges which are directly linked to the amplitude and phase of each component within the measured signal. The properties of such a representation applied to asymptotic frequency modulated signals have been studied extensively since 1990 [7–13]. From the extraction of the ridges and from the value of the CWT along the ridges, modal parameters are identified. This procedure can be seen as an isolation of a mode of vibration: the identification procedure is then easier because it is performed on the amplitude and phase of one component of the measured signal separately as it is for a single-degree-of-freedom (s.d.o.f) system.

Some authors have already used wavelet analysis processing free responses of mechanical structures in order to identify their modal characteristics. Staszewski [14] proposed three methods for estimating modal damping ratios based on the CWT. Ruzzene et al. [15] showed that the CWT applied to free responses of m.d.o.f system represents a consistent improvement for the estimation of instantaneous frequencies compared to the Hilbert transform (HT). These authors used the Morlet wavelet and the identification of the mode shapes is not performed. Argoul et al. [16–18] chose the Cauchy wavelet and provided a procedure to identify natural frequencies and viscous damping ratios as well mode shapes. The previous authors applied their identification techniques to proportionally damped m.d.o.f systems. Newland [19–21] introduced a new orthogonal wavelet called harmonic wavelet. Tang [22] used this mother wavelet to process exponentially time-decaying signals in a relatively narrow bandwith situation. Most of these authors applied their procedure to real data [15–18,21,22]. Finally, Staszewski [23] and Argoul and Le [18] started to adapt their procedure to non-linear systems.

In light of these references, the choice of the mother wavelet is not obvious; in addition, the value of the parameter(s) appearing in its definition is not clearly explained. For the numerical computation of the CWT of finite record signals, the problem of the edge effect is sometimes seen but not seriously tackled. Moreover, damping estimation is only performed from the modulus of the CWT.

The aim of this paper is to improve the use of continuous wavelet transform for modal identification purposes from the free-decay responses of structures. The choice of the mother wavelet and of its localization properties is discussed. Efforts are made to remedy the problem of edge effect appearing during the numerical computation of the CWT. The procedure of identification of the modal characteristics (modal frequencies, modal damping ratios and mode shapes) based on the CWT (modulus and phase) is presented in detail.

The paper is arranged as follows: Section 2 provides a description of the general theoretical background on CWT, and develops its application to frequency modulated signals. Section 3 is devoted to the formulation of the modal parameters identification, in which the relations between the data and the modal parameters are given. Numerical and practical aspects of this procedure are studied in Section 4. The approach is to process the edge effect problem and to propose some rules for the choice of the mother wavelet's parameters. The step-by-step algorithm for the procedure is then presented. The final section (Section 5) illustrates the edge effect and validates the procedure with a numerical example.

## 2. CWT applied to frequency modulated signals

### 2.1. Continuous wavelet transform: theoretical background

For the sake of completeness, this section gives a basic presentation of the wavelet transform theory together with the most relevant properties for the proposed procedure. The same definition as used by Carmona et al. [11] is chosen for the CWT of a signal $u(t)$, that is a finite energy and piece-wise continuous function of $t$,

$$T_\psi[u](b,a) = \frac{1}{a}\int_{-\infty}^{+\infty} u(t)\bar{\psi}\left(\frac{t-b}{a}\right)\mathrm{d}t, \tag{1}$$

where $\psi(.)$ is a square integrable and piece-wise continuous function called the mother or analyzing wavelet, and $\bar{\psi}(.)$ is its complex conjugate. The pair $(b,a)$ is called the time-scale variable of the analysis, where $a$ ($a>0$) is a scale parameter that plays the role of the inverse of frequency, and $b$ is a translation parameter related to time. Eq. (1) can be viewed as either the inner product between the signal $u(t)$ and the shifted and scaled copies of $\psi(t):\psi_{b,a}(t)=(1/a)\psi((t-b)/a)$, or as the convolution product between $u(t)$ and $(1/a)\bar{\psi}\left(-\frac{\cdot}{a}\right)$. The function $\psi(t)$ is an admissible mother wavelet when $C_\psi$, defined by

$$C_\psi = \int_0^{+\infty} |\hat{\psi}(a\omega)|^2 \frac{\mathrm{d}a}{a}, \tag{2}$$

is finite, non-zero and independent of the real number $\omega$. In Eq. (2), $\hat{\psi}(\omega)$ is the Fourier transform (FT) of $\psi(t):\hat{\psi}(\omega)=\int_{-\infty}^{+\infty}\psi(t)\mathrm{e}^{-\mathrm{i}\omega t}\,\mathrm{d}t$. When this admissibility condition is verified, the signal $u(t)$ can be reconstructed by

$$u(t) = \frac{1}{C_\psi}\int_{-\infty}^{+\infty}\int_0^{+\infty} T_\psi[u](b,a)\psi\left(\frac{t-b}{a}\right)\frac{\mathrm{d}a}{a}\,\mathrm{d}b. \tag{3}$$

Moreover, Parseval's theorem applied to Eq. (1) gives the following expression in frequency domain:

$$T_\psi[u](b,a) = \frac{1}{2\pi}\int_{-\infty}^{+\infty} \hat{u}(\omega)\bar{\hat{\psi}}(a\omega)\mathrm{e}^{\mathrm{i}\omega b}\,\mathrm{d}\omega. \tag{4}$$

The local resolution of the CWT in time and in frequency depends on the dilatation parameter $a$ and is determined, respectively, by the duration $\Delta t_\psi$ and bandwidth $\Delta\omega_\psi$ of the mother wavelet:

$$\Delta t = a\Delta t_\psi, \qquad \Delta\omega = \frac{\Delta\omega_\psi}{a}. \tag{5}$$

Here, $\Delta t_\psi$ and $\Delta\omega_\psi$ are stated in terms of root mean squares [24] which are equivalent to standard deviations in statistics

$$\Delta t_\psi = \frac{1}{||\psi||_2}\sqrt{\int_{-\infty}^{+\infty}(t-t_\psi)^2|\psi(t)|^2\,\mathrm{d}t}, \tag{6}$$

$$\Delta\omega_\psi = \frac{1}{||\hat{\psi}||_2}\sqrt{\int_{-\infty}^{+\infty}(\omega-\omega_\psi)^2|\hat{\psi}(\omega)|^2\,\mathrm{d}\omega}, \tag{7}$$

where $t_\psi$ and $\omega_\psi$ are the centre of $\psi(t)$ and $\hat{\psi}(\omega)$, respectively,

$$t_\psi = \int_{-\infty}^{+\infty} t\frac{|\psi(t)|^2}{||\psi||_2^2}\,\mathrm{d}t \quad \text{and} \quad \omega_\psi = \int_{-\infty}^{+\infty}\omega\frac{|\hat{\psi}(\omega)|^2}{||\hat{\psi}||_2^2}\,\mathrm{d}\omega. \tag{8}$$

$||\cdot||_2$ denotes the classical norm in the space of square integrable functions. The function $\psi$ is said to be localized about the phase point $(t_\psi,\omega_\psi)$ with uncertainty $\mu(\psi)=\Delta t_\psi\Delta\omega_\psi$. It can be seen from Eq. (5) that $\mu(\psi_{b,a})=\Delta t\Delta\omega=\mu(\psi)$. The Heisenberg uncertainty principle states that $\mu(\psi)\geqslant\frac{1}{2}$; thus, an improvement of the time localization (i.e., a decrease of $\Delta t$) is accompanied by a deterioration in the frequency localization (i.e., an increase of $\Delta\omega$). If $\omega_\psi/a$ is considered to be the frequency variable $\omega$, then the $t\omega$ plane can be viewed as the time–frequency plane. The localization domain for the CWT at point $(b,\omega=\omega_\psi/a)$ becomes

$$[b+at_\psi-a\Delta t_\psi, b+at_\psi+a\Delta t_\psi]\times\left[\frac{\omega_\psi}{a}-\frac{\Delta\omega_\psi}{a},\frac{\omega_\psi}{a}+\frac{\Delta\omega_\psi}{a}\right]. \tag{9}$$

Referring to the conventional frequency analysis of constant-$Q$ filters, the $Q$ factor is introduced as the ratio of the centre-frequency to the frequency bandwidth

$$Q = \frac{\omega_\psi/a}{2(\Delta\omega_\psi/a)} = \frac{\omega_\psi}{2\Delta\omega_\psi}. \tag{10}$$

$Q$ is independent of $a$. Gram-Hansen and Dorize [25] associate this $Q$ value to the filter bank of a $(1/N)$th octave that is a classical notion in acoustics: a $(1/N)$th octave band of centre frequency $\omega_\psi$ is a band $[\omega_1,\omega_2]$ with $\omega_1=2^{-1/(2N)}\omega_\psi$ and $\omega_2=2^{1/(2N)}\omega_\psi$, hence $Q=1/2^{1/(2N)}-2^{-1/(2N)}$.

Due to the linearity property of the CWT, the signal of multi-components can be processed as

$$T_\psi\left[\sum_{j=1}^{N} u_j\right](b,a) = \sum_{j=1}^{N} T_\psi[u_j](b,a). \tag{11}$$

Using localization properties of the mother wavelets, in both time and frequency domains, a particular component $u_j$ can be extracted from multi-component signals. If $\psi$ and $u$ are continuous and piece-wise differentiable, the integration by parts theorem allows relation (1) to be rewritten as

$$T_\psi[\dot{u}](b,a) = \frac{1}{a}\left[u(t)\bar{\psi}\left(\frac{t-b}{a}\right)\Big|_{-\infty}^{+\infty} - \frac{1}{a}\int_{-\infty}^{+\infty} u(t)\dot{\bar{\psi}}\left(\frac{t-b}{a}\right)\mathrm{d}t\right]. \tag{12}$$

Moreover, when $\dot{\psi}$ is square and absolutely integrable and $\dot{u}$ is of finite energy, the CWT of $\dot{u}$ with $\psi$ is then related to the CWT of $u$ with $\dot{\psi}$:

$$T_\psi[\dot{u}](b,a) = -\frac{1}{a}\,T_{\dot{\psi}}[u](b,a). \tag{13}$$

This relation can be easily extended to the finite energy signal $\ddot{u}$ when $\ddot{\psi}$ is square and absolutely integrable:

$$T_\psi[\ddot{u}](b,a) = -\frac{1}{a}\,T_{\dot{\psi}}[\dot{u}](b,a) = \frac{1}{a^2}\,T_{\ddot{\psi}}[u](b,a). \tag{14}$$

It should be also noted that for the expression of $T_{\dot{\psi}}[\dot{u}]$ and of $T_{\ddot{\psi}}[u]$ in the frequency domain [see Eq. (4)], $\hat{\dot{\psi}}(\omega)$ and $\hat{\ddot{\psi}}(\omega)$ can be substituted by $-\mathrm{i}\omega\hat{\psi}(\omega)$ and $-\omega^2\hat{\psi}(\omega)$, respectively.

### 2.2. CWT of frequency modulated signals and ridge estimation

A finite energy real signal $u(t)$ can always be associated with an *analytic signal* $Z_u(t)$ by making use of the Hilbert transform:

$$Z_u(t) = [I + \mathrm{i}H]u(t), \tag{15}$$

where $I$ and $H$ are, respectively, the identity and the Hilbert transform operators. It gives

$$\begin{aligned} \hat{Z}_u(\omega) &= 2\Theta(\omega)\hat{u}(\omega), \\ u(t) &= \mathrm{Re}[Z_u(t)], \end{aligned} \tag{16}$$

where $\Theta$ denotes the Heaviside function. One defines the *canonical pair* $(A_u(t), \phi_u(t))$ of signal $u(t)$ with modulus $A_u(t) = |Z_u(t)|$ $(A_u(t) \geqslant 0)$ and phase $\phi_u(t) = \angle[Z_u(t)]$ $(\phi_u(t) \in [0, 2\pi))$; hence $u(t) = A_u(t)\cos(\phi_u(t))$. The instantaneous angular frequency $\omega_u(t)$ is then given by

$$\omega_u(t) = \frac{\mathrm{d}\phi_u(t)}{\mathrm{d}t} = \dot{\phi}_u(t). \tag{17}$$

This canonical representation has proved to be useful in many applications. However, when multi-component signals are under study, a band-pass filtering is necessary in order to separate each component.

Conversely, when $u(t)$ is given in the form of a single component

$$u(t) = A(t)\cos(\phi(t)), \tag{18}$$

its analytical signal $Z_u(t)$ is generally different from the associated complex signal $A(t)e^{i\phi(t)}$. $Z_u(t)$ can be approximated by $A(t)e^{i\phi(t)}$:

$$Z_u(t) \approx A(t)e^{i\phi(t)}, \tag{19}$$

and $u(t)$ is then called an *asymptotic signal* if it is sufficiently "oscillatory". This approximation means that the oscillations resulting from the phase term $\phi(t)$ are much faster than the variation coming from the amplitude term $A(t)$. When the admissible mother wavelet $\psi(t)$ is progressive (i.e its Fourier transform $\hat{\psi}(\omega)$ vanishes for $\omega \leqslant 0$), the CWT of a real-valued signal $u$ is related to the CWT of its analytical signal $Z_u(t)$

$$T_\psi[u](b,a) = \langle u, \psi_{b,a}(t)\rangle = \frac{1}{2}\langle Z_u, \psi_{b,a}(t)\rangle = \frac{1}{2}T_\psi[Z_u](b,a). \tag{20}$$

The main feature of the CWT applied to asymptotic signals is that it is concentrated along curves in the time–frequency domain called "ridges". The restriction of the wavelet transform to each ridge, called the "skeleton" of the transform, contains a maximal information: it is very close to the component of the signal itself. A definition of the ridge and an approximation of the skeleton are given in Refs. [7–13] as

$$a_r(b) = \frac{K}{\dot{\phi}_u(b)}, \tag{21}$$

$$T_\psi[u](b, a_r(b)) \approx Corr(b)Z_u(b), \tag{22}$$

where $K$ is a constant depending on the mother wavelet and $Corr(b)$ is the correction function entirely characterized by the mother wavelet and by the ridge $a_r(b)$. Once the ridge is determined, the analytical signal $Z_u(t)$ can be deduced. Its real and imaginary parts give the signal and its Hilbert transform, respectively. The ridge extraction is obtained through a non-parametric identification technique, for which several algorithms can be found in Refs. [7–13]. "Differential" methods are based on a local analysis of either the extrema of the CWT modulus, or the points where the frequency of the CWT coincides with that of the scaled wavelet. In "integral" methods, ridges are seen as smooth and slowly varying functions where the energy has a tendency to localize in the time–frequency map. An appropriate penalty function is then optimized for obtaining the set of smooth ridge candidates. The choice of a method, either differential or integral, strongly depends on noisy or clean signals. Due to the pure signals processed in this paper, the *Marseille method* [7,9,11] is applied. The phase of the CWT is used with $K = \dot{\phi}_\psi(0)$ and $Corr(b) = \hat{\psi}(a_r\dot{\phi}_u(b))$, where $\phi_\psi(t)$ denotes the phase of the mother wavelet. If significant noise is present within the signal, integral methods, which are more stable than differential ones, are recommended. For instance, Staszewski [23] uses the simulated annealing algorithm to minimize the penalty function.

## 3. Formulating modal parameters identification

### 3.1. Free responses of viscous damped modal m.d.o.f system

Consider a m.d.o.f mechanical system with viscous proportional damping. The free responses at point $k$ of such a system of $N$ degrees of freedom, in terms of displacement $u_k(t)$, velocity $\dot{u}_k(t)$ and acceleration $\ddot{u}_k(t)$, are expressed according to the modal basis

$$u_k(t) = \sum_{j=1}^{N} u_{kj}(t) = \sum_{j=1}^{N} \Phi_{kj}\rho_j e^{-\xi_j\omega_j t}\cos(\tilde{\omega}_j t - \varphi_j), \tag{23}$$

$$\dot{u}_k(t) = \sum_{j=1}^{N} \dot{u}_{kj}(t) = -\sum_{j=1}^{N} \Phi_{kj}\rho_j\omega_j e^{-\xi_j\omega_j t}\cos(\tilde{\omega}_j t - \varphi_j - \delta_j), \tag{24}$$

$$\ddot{u}_k(t) = \sum_{j=1}^{N} \ddot{u}_{kj}(t) = -\sum_{j=1}^{N} \Phi_{kj}\rho_j\omega_j^2 e^{-\xi_j\omega_j t}\cos(\tilde{\omega}_j t - \varphi_j + \theta_j), \tag{25}$$

where $j$ is the mode number. $\Phi_{kj}$ is the $(k,j)$ term of the modal matrix made of eigenvectors $\Phi_j = [\Phi_{1j}, \Phi_{2j}, \ldots \Phi_{Nj}]^{\mathrm{T}}$. Each of these vectors can be normalized to give the maximum value $\Phi_{mj}$ equal to unity. For the mode $j$: $\omega_j$, $\tilde{\omega}_j$ are the undamped and damped vibration angular frequencies and $\xi_j$ is the damping ratio

$$\rho_j = \left\{ \left[ \frac{\dot{Y}_j(0) + \xi_j\omega_j Y_j(0)}{\tilde{\omega}_j} \right]^2 + [Y_j(0)]^2 \right\}^{1/2},$$

$Y_j(0)$ and $\dot{Y}_j(0)$ are the initial modal displacement and velocity of mode $j$; $\varphi_j = \arctan\left\{(c_{j0} + \xi_j)/\sqrt{1-\xi_j^2}\right\}$ with $c_{j0} = \dot{Y}_j(0)/(\omega_j Y_j(0))$, $\delta_j = \arctan\left\{\sqrt{1-\xi_j^2}/\xi_j\right\}$ and $\theta_j = \arctan\left\{2\xi_j\sqrt{1-\xi_j^2}/(1-2\xi_j^2)\right\}$.

Relations (23), (24) and (25) can be rewritten in general form: $\sum_{j=1}^{N} A_{kj}(t)\cos(\alpha_{kj}(t))$ where

$$\begin{cases} \alpha_{u_{kj}}(t) = \tilde{\omega}_j t - \varphi_j + \dfrac{\pi}{2}(1 - \mathrm{sgn}(\Phi_{kj})), & \text{(a)} \\ A_{u_{kj}}(t) = |\Phi_{kj}|\rho_j e^{-\xi_j\omega_j t} \text{ for } u_k(t), & \text{(b)} \end{cases} \tag{26}$$

$$\begin{cases} \alpha_{\dot{u}_{kj}}(t) = \tilde{\omega}_j t - \varphi_j - \delta_j + \dfrac{\pi}{2}(1 + \mathrm{sgn}(\Phi_{kj})), & \text{(a)} \\ A_{\dot{u}_{kj}}(t) = |\Phi_{kj}|\rho_j\omega_j e^{-\xi_j\omega_j t} \text{ for } \dot{u}_k(t), & \text{(b)} \end{cases} \tag{27}$$

$$\begin{cases} \alpha_{\ddot{u}_{kj}}(t) = \tilde{\omega}_j t - \varphi_j + \theta_j + \dfrac{\pi}{2}(1 + \mathrm{sgn}(\Phi_{kj})), & \text{(a)} \\ A_{\ddot{u}_{kj}}(t) = |\Phi_{kj}|\rho_j\omega_j^2 e^{-\xi_j\omega_j t} \text{ for } \ddot{u}_k(t). & \text{(b)} \end{cases} \tag{28}$$

The assumption of weak damping is made; thus, it is shown in Ref. [26] that each component of these signals is asymptotic when $\xi_j \ll 1/\sqrt{2}$: $Z_{kj}(t) \approx A_{kj}(t)e^{i\alpha_{kj}(t)}$. Moreover, Géradin and Rixen [27] show that in the case of non-proportional damping, the assumption of weak damping allows

the off-diagonal terms in the generalized damping matrix to be neglected without disturbing significantly (through second order perturbation) the spectrum of eigenvalues of the damped system.

### 3.2. Relations between data and modal parameters

The data for the modal identification come in the form of instantaneous functions: the amplitude $A_{u_{kj}}(t)$ (or $A_{\dot{u}_{kj}}(t)$ or $A_{\ddot{u}_{kj}}(t)$), and the phase $\alpha_{u_{kj}}(t)$ (or $\alpha_{\dot{u}_{kj}}(t)$ or $\alpha_{\ddot{u}_{kj}}(t)$) of each component extracted from the CWT of the measured free responses $u_k(t)$ (or $\dot{u}_k(t)$ or $\ddot{u}_k(t)$) at point $k$. Simple instantaneous relations $R(t)$ between data and modal parameters are deduced from Eqs. (26), (27) and (28) in order to get linear or constant relations. The estimation of modal parameters is then performed through a parametric identification technique based on the minimization by the least-squares method of an error criterion defined as the difference between the instantaneous functions that are derived from the measurement $R^{measure}(t)$ and those obtained with the model $R^{model}(t)$.

(1) *Use of phases*: The time evolution of the phase $\alpha_{u_{kj}}(t)$ (or $\alpha_{\dot{u}_{kj}}(t)$ or $\alpha_{\ddot{u}_{kj}}(t)$) given in Eq. (26a) (or (27a), or (28a)) is a straight line with slope $\tilde{\omega}_j$; the estimation of $\tilde{\omega}_j$ leads then to a straight line inverse problem. The time evolution of the ridge $a_{r_{u_{kj}}}(t)$ given in Eq. (21), gives:

$$\tilde{\omega}_j = \dot{\alpha}_{u_{kj}} = \frac{K}{a_{r_{u_{kj}}}(t)}, \tag{29}$$

$$\text{or} \quad \tilde{\omega}_j = \dot{\alpha}_{\dot{u}_{kj}}(t) = \frac{K}{a_{r_{\dot{u}_{kj}}}(t)}, \tag{30}$$

$$\text{or} \quad \tilde{\omega}_j = \dot{\alpha}_{\ddot{u}_{kj}}(t) = \frac{K}{a_{r_{\ddot{u}_{kj}}}(t)}. \tag{31}$$

Two other relations based on the phase give the damping ratio directly

$$\xi_j = |\cos(\delta_j - \pi \operatorname{sgn}(\Phi_{kj}))| = |\cos(\alpha_{u_{kj}}(t) - \alpha_{\dot{u}_{kj}}(t))|,$$

$$\text{or} \quad \xi_j = \left|\cos\left(\frac{\theta_j + \pi \operatorname{sgn}(\Phi_{kj})}{2}\right)\right| = \left|\cos\left(\frac{\alpha_{\ddot{u}_{kj}}(t) - \alpha_{u_{kj}}(t)}{2}\right)\right|. \tag{32}$$

The phase difference $d_j^{kl}(t)$ of the mode $j$ between point $k$ and point $l$:

$$d_j^{kl}(t) = \alpha_{u_{kj}}(t) - \alpha_{u_{lj}}(t) = -(\alpha_{\dot{u}_{kj}}(t) - \alpha_{\dot{u}_{lj}}(t)) = -(\alpha_{\ddot{u}_{kj}}(t) - \alpha_{\ddot{u}_{lj}}(t)) \tag{33}$$

is either null or equal to $\pm\pi$

$$d_j^{kl}(t) = \frac{\pi}{2}(\operatorname{sgn}(\Phi_{lj}) - \operatorname{sgn}(\Phi_{kj})). \tag{34}$$

Thus, $\Phi_{kj}$ and $\Phi_{lj}$ have the same sign if $d_j^{kl}(t) = 0$ and opposite signs if $d_j^{kl}(t) = \pm\pi$.

(2) *Use of amplitudes*: $\omega_j$ can be expressed as

$$\omega_j = \frac{A_{\dot{u}_{kj}}(t)}{A_{u_{kj}}(t)} \quad \text{or} \quad \omega_j = \frac{A_{\ddot{u}_{kj}}(t)}{A_{\dot{u}_{kj}}(t)}. \tag{35}$$

The time evolution of the logarithm of amplitude $\log(A_{u_{kj}}(t))$ (or $\log(A_{\dot{u}_{kj}}(t))$ or $\log(A_{\ddot{u}_{kj}}(t))$) is a straight line with slope $-\xi_j\omega_j$, as seen below

$$\begin{aligned}\log(A_{u_{kj}}(t)) &= \log(|\Phi_{kj}|\rho_j) - \xi_j\omega_j t,\\ \log(A_{\dot{u}_{kj}}(t)) &= \log(|\Phi_{kj}|\rho_j\omega_j) - \xi_j\omega_j t,\\ \log(A_{\ddot{u}_{kj}}(t)) &= \log(|\Phi_{kj}|\rho_j\omega_j^2) - \xi_j\omega_j t.\end{aligned} \tag{36}$$

The identification problem is again a straight line inverse problem. The ratio $A_{u_{kj}}(t)/A_{u_{mj}}(t)$ of the amplitude of the $j$th component of the response at point $k$ upon that at point $m$ is a constant in time which is the absolute value of the $k$th component of mode $j$; thus,

$$\frac{|\Phi_{kj}|}{|\Phi_{mj}|} = |\Phi_{kj}| = \frac{A_{u_{kj}}(t)}{A_{u_{mj}}(t)}. \tag{37}$$

## 4. Numerical and practical aspects of CWT

### 4.1. Mother wavelet choice

The optimal mother wavelet $\psi$ for modal identification purposes using the free responses of a m.d.o.f system should satisfy the following conditions: (a) $\psi$ is admissible (Eq. (2)). (b) $\psi$ is progressive. (c) $\psi$ has good time and frequency localization properties. (d) The first and the second derivatives of $\psi$ satisfy the three previous conditions, and thus Eq. (14) can be used.

The first condition is obvious. Several reasons suggest the use of progressive wavelets instead of real ones for the analysis of real signals (cf. Ref. [11]): (i) it allows the direct connection between a real signal and its associated analytic signal (see Eq. (20)). (ii) the wavelet transform of real signals using real wavelets yields real wavelet coefficients, and there is no natural way of making a connection with some "local spectrum" which one would like associate with a given signal. The third condition is very important in the context of time–frequency analysis and the final condition makes the processing by CWT of displacement, velocity and acceleration easier without differential and integral operations.

Three complex-valued mother wavelets are compared. One or two parameters appear in the definition of each mother wavelet and strongly influence the localization properties. The first one is the well-known Morlet wavelet. The second is the Cauchy wavelet of order $n$, intensively used in quantum mechanics [28] when $n = 1$ and also by Argoul et al. [16–18,29] when $n > 1$. Finally, the third one is the harmonic wavelet recently proposed by Newland [19–21]. The formulae of $\psi(t)$, $\hat{\psi}(\omega)$, $C_\psi$, $t_\psi$, $\omega_\psi$, $\Delta t_\psi$, $\Delta\omega_\psi$, $\mu_\psi$ and $Q$ are given in Table 1 for the three wavelets. The first and the second condition are verified by both Cauchy and harmonic wavelets. The Morlet wavelet is only numerically admissible and progressive when the product of the two parameters $\beta\delta$ is large enough ($(\beta\delta) \geqslant 5$ in practice). According to the third condition, the Morlet wavelet has its time–frequency window with the smallest area allowable $\left(\frac{1}{2}\right)$ by the Heisenberg inequality. The uncertainty $\mu_\psi$ of the Cauchy wavelet behaves asymptotically with this threshold when its order parameter $n$ tends towards infinity. The harmonic wavelet has infinite uncertainty but its support in frequency domain is compact. This property allows the isolation of components with close frequencies. Newland [21] improves time localization by windowing the spectrum of wavelets, but it is more complicated. The last condition is easily verified by the definition of the Cauchy wavelet

Table 1
Definition of the main characteristics of the three mother wavelets

| | Morlet wavelet | Cauchy wavelet | Harmonic wavelet[a] |
|---|---|---|---|
| $\psi(t)$ | $e^{-t^2/(2\delta^2)}e^{i\beta t}$ | $\left(\frac{i}{t+i}\right)^{n+1}$ | $\frac{e^{i2m\pi t}-e^{i2m\pi t}}{i2\pi(n-m)t}$ |
| $\hat{\psi}(\omega)$ | $\delta\sqrt{2\pi}e^{-(\omega-\beta)^2\delta^2/2}$ | $\frac{2\pi\omega^n e^{-\omega}}{n!}\Theta(\omega)$ | $\frac{\Theta[(\omega-m2\pi)(n2\pi-\omega)]}{(n-m)2\pi}$ |
| $C_\psi$: | $\infty$ | $4\pi^2\frac{1}{2^{2n}}\frac{(2n-1)!}{(n!)^2}$ | $\frac{1}{4\pi^2(n-m)^2}\ln\left(\frac{n}{m}\right)$ |
| $t_\psi$ | 0 | 0 | 0 |
| $\omega_\psi$ | $\beta$ | $n+\frac{1}{2}$ | $(n+m)\pi$ |
| $\Delta\omega_\psi$: | $\frac{1}{\delta\sqrt{2}}$ | $\frac{\sqrt{2n+1}}{2}$ | $(n-m)\pi$ |
| $\Delta t_\psi$: | $\frac{\delta}{\sqrt{2}}$ | $\frac{1}{\sqrt{2n-1}}$ | $\infty$ |
| $\mu_\psi$: | $\frac{1}{2}$ | $\frac{1}{2}\sqrt{1+\frac{2}{2n-1}}$ | $\infty$ |
| $Q=\frac{\omega_\psi}{2\Delta\omega_\psi}$ | $\frac{\beta\delta}{\sqrt{2}}$ | $\frac{n+\frac{1}{2}}{\sqrt{2n+1}}$ | $\frac{(n+m)}{2(n-m)}$ |

[a] Newland uses the inverse FT definition: $w(x)=\int_{-\infty}^{+\infty}\hat{w}(\omega)e^{i\omega x}\,d\omega$.

given in Table 1. The first and the second derivatives of $\psi_n$ are also the Cauchy wavelets since

$$\dot{\psi}_n(t)=i(n+1)\psi_{n+1}(t) \quad \text{and} \quad \ddot{\psi}_n(t)=-(n+1)(n+2)\psi_{n+2}(t), \tag{38}$$

and the identification procedure with $\dot{u}$ and $\ddot{u}$ by the aid of Eq. (14) can be simplified. The first and second derivatives of the Morlet wavelet also satisfy the fourth condition, but they are not the Morlet wavelets and their time–frequency localization are no longer as good as the Morlet wavelet [26]. The derivatives of the harmonic wavelet are admissible and progressive, however, its time localizations are poor; moreover they are not absolutely integrable, so the application of Eq. (14) is limited.

The properties of the mother wavelet can be referred to the parameter $Q$ defined in relation (10) [30]. To compare the three proposed mother wavelets, the $Q$ factor is used: each mother wavelet will have the same value of $Q$ and $\omega_\psi$ (and consequently the same $\Delta\omega_\psi$). Each mother wavelet and its corresponding FT are plotted in Fig. 1 according to different values of $(1/N)$th octave which is

Fig. 1. Modulus of mother wavelets in time and in frequency domains corresponding to different $Q$ values: (a) $Q=1.4142$ (1 octave), (b) $Q=17.3099$ (1/12 octave). Cauchy wavelet: ○, Morlet wavelet: ∗ and harmonic wavelet: △. Vertical lines - - - delimit $I_{c_t}$ and $I_{c_f}$ [see Section 4.2].

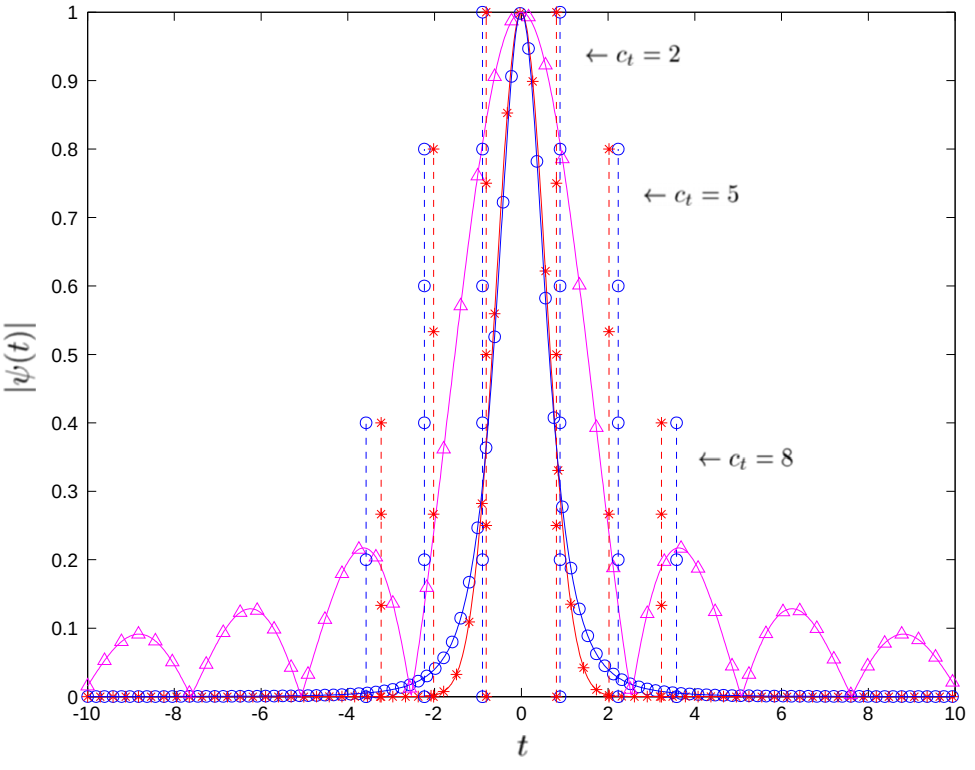
$|\psi(t)|$
$\leftarrow c_t = 2$
$\leftarrow c_t = 5$
$\leftarrow c_t = 8$
$t$

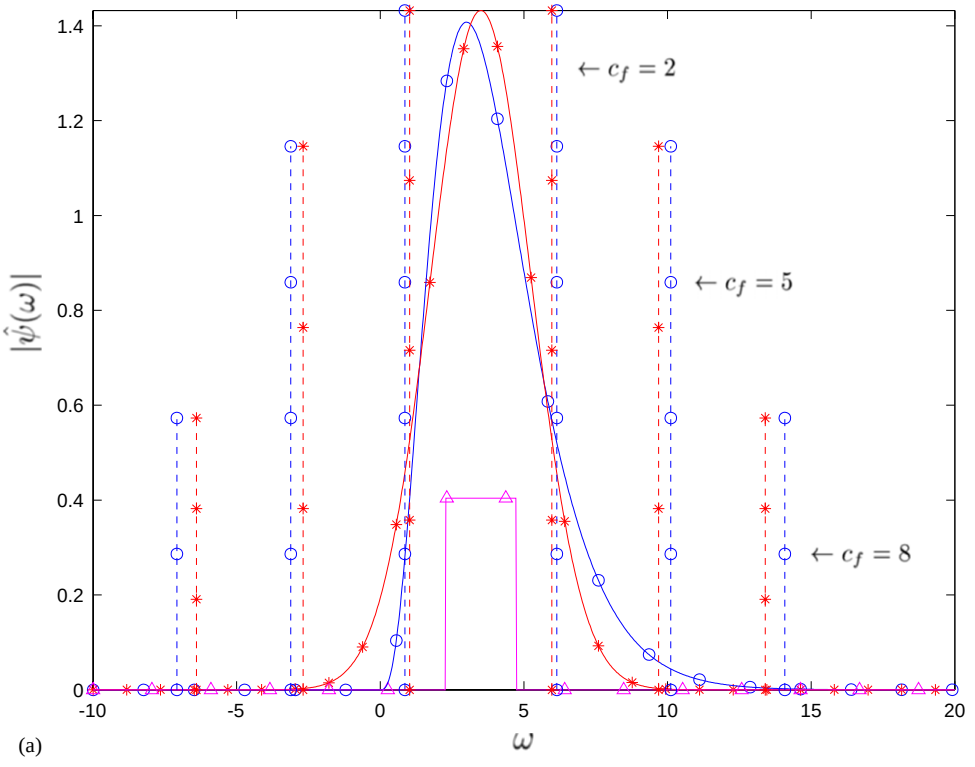
$|\hat{\psi}(\omega)|$
$\leftarrow c_f = 2$
$\leftarrow c_f = 5$
$\leftarrow c_f = 8$
$\omega$

(a)

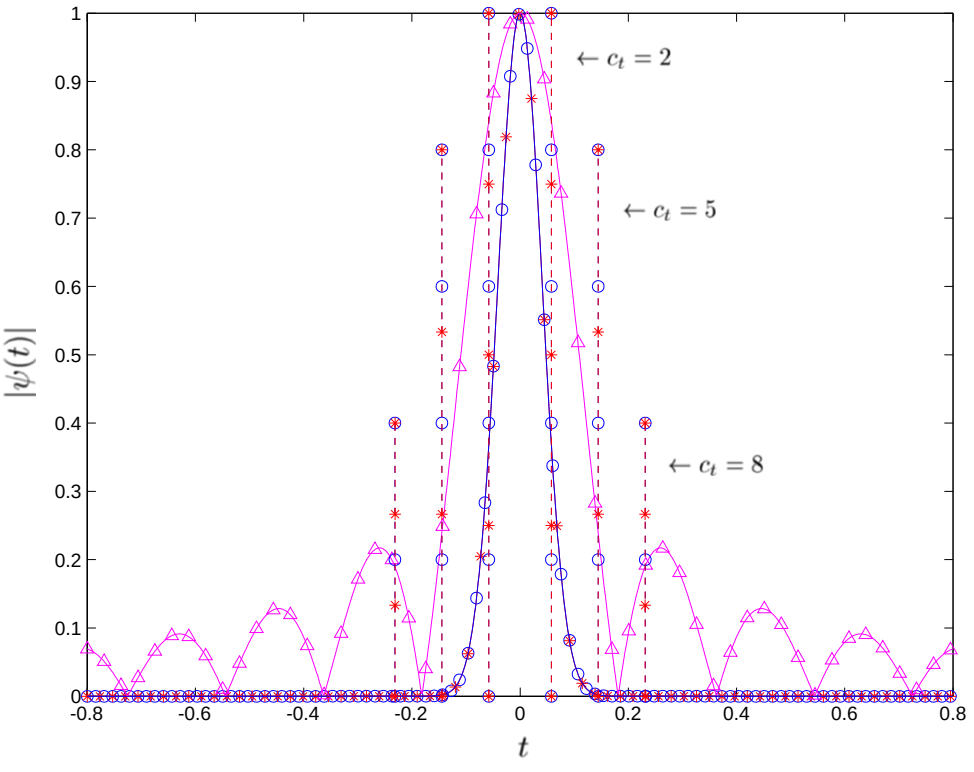


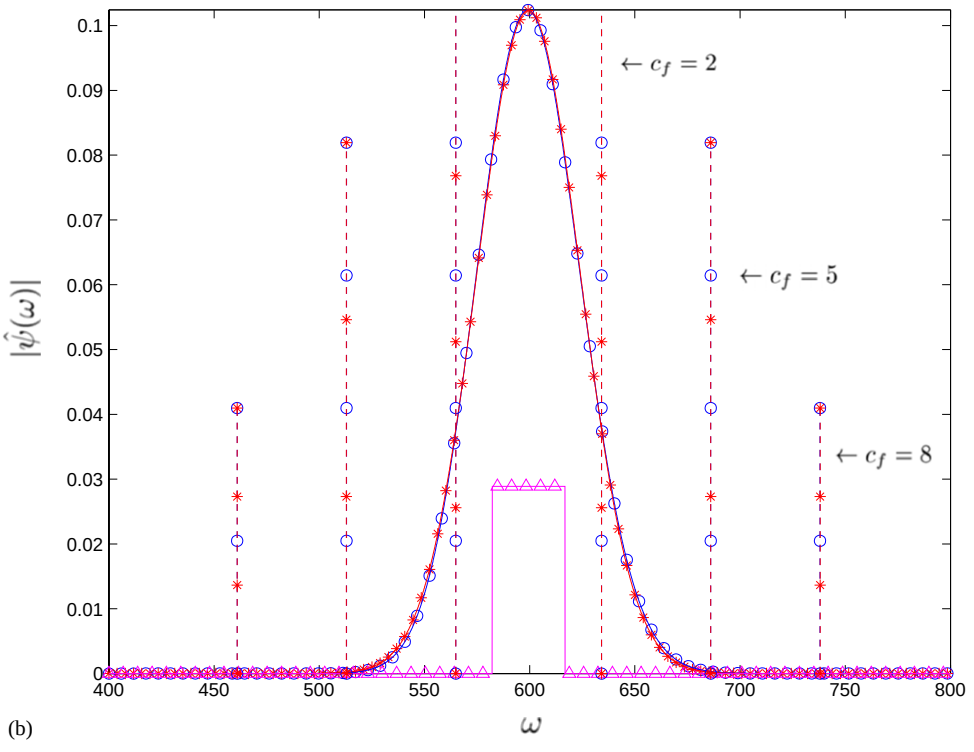


(b)

Fig. 1 (*continued*).

Table 2
Dependence of the definition parameters of the three mother wavelets on $Q$

| Filter | | Morlet wavelet | | Cauchy wavelet | Harmonic wavelet | |
|---|---|---|---|---|---|---|
| Octave | Q | $\beta$ | $\delta$ | $n$ | $n$ | $m$ |
| 1 | 1.4142 | 3.5 | 0.5714 | 3 | 0.7540 | 0.3601 |
| 1/3 | 4.3185 | 37.5 | 0.1629 | 37 | 6.6593 | 5.2773 |
| 1/6 | 8.6514 | 149.5 | 0.0818 | 149 | 25.1688 | 22.4185 |
| 1/12 | 17.3099 | 559.5 | 0.0408 | 559 | 98.1694 | 92.6574 |

directly linked to $Q$ [see Section 2.1]. Table 2 gives $N$, $Q$ and the correspondence between the definition parameters of each mother wavelet. Some remarks follow:

(i) for the Morlet wavelet, $\hat{\psi}(0)\neq 0$ but $\hat{\psi}(0)$ tends towards 0 when the product $\beta\delta$ increases, moreover, at a given $\omega_j$, the localizations in time and in frequency obtained from Eq. (5) and Table 1: $\Delta t_{\omega_j} = \beta\delta/(\omega_j\sqrt{2})$ and $\Delta\omega_{\omega_j} = \omega_j/(\beta\delta\sqrt{2})$ depend only on the product $\beta\delta$ and thus on $Q$ value. So, without loss of generality, one can assign $\delta = 1$ and $\beta$ varying to reach the expected value of $Q$. (ii) The more $Q$ increases, the closer the Cauchy and the Morlet wavelet curves become in the both time and frequency domains. (iii) The harmonic wavelet has very poor properties in time and exhibits the Gibbs phenomenon because of discontinuties in the frequency domain. In addition, the harmonic wavelet is not absolutely integrable which is required for a window function in practical purposes [24]. Thus, the CWT computed with harmonic wavelet will not be retained for the modal identification purpose, which agrees with the conclusion of Tang [22] when he compares it to short time Fourier transform. (iv) when $Q$ is small ($\beta\delta = \beta < 5$, i.e, $Q < 5/\sqrt{2}$ in practice), it is natural to use the Cauchy wavelet instead of the Morlet wavelet and when $Q \geqslant 5/\sqrt{2}$ (i.e $\beta\delta = \beta \geqslant 5$ and $n \geqslant 25$), the Cauchy wavelet has uncertainty $\mu_\psi \sim \frac{1}{2}(1 + 1/(2n-1) + o(1/(2n-1))^2)$. It shows that the variation of $\mu_\psi$ versus $Q$ tends quickly toward $\frac{1}{2}$ when $Q$ increases; this variation is presented in Fig. 2. Because the difference in time–frequency localization between the Cauchy and Morlet wavelets is less than 2%, it is still possible to use the Cauchy wavelet.

### 4.2. CWT computation-edge effect

The measured signal $u(t)$ is generally sampled over the finite length record $L$ with a sampling period $T$. The frequency content of this discrete version is limited by the Nyquist frequency $f_{Nyquist} = 1/(2T)$. The CWT computation can be performed by different algorithms: quadrature rule, fast Fourier transform (FFT) with or without zero padding, convolution product and the chirp Z transform [26]. As the definition of the CWT given by Eq. (1) consists of an integration over all $\mathbb{R}$, the signal can be either put to zero outside the record interval or periodized by FFT algorithm. All examples in the following will be performed with FFT algorithm implemented in MATLAB software.

The edge-effect problem, well described by Slavic et al. [31], arises due to the finite length and to the discretization of measured data record and to the nature of the CWT (convolution product see Section 2.1). It cannot be removed and a domain $D$ in the $t\omega$ plane, where the edge effect can be neglected, can be determined.

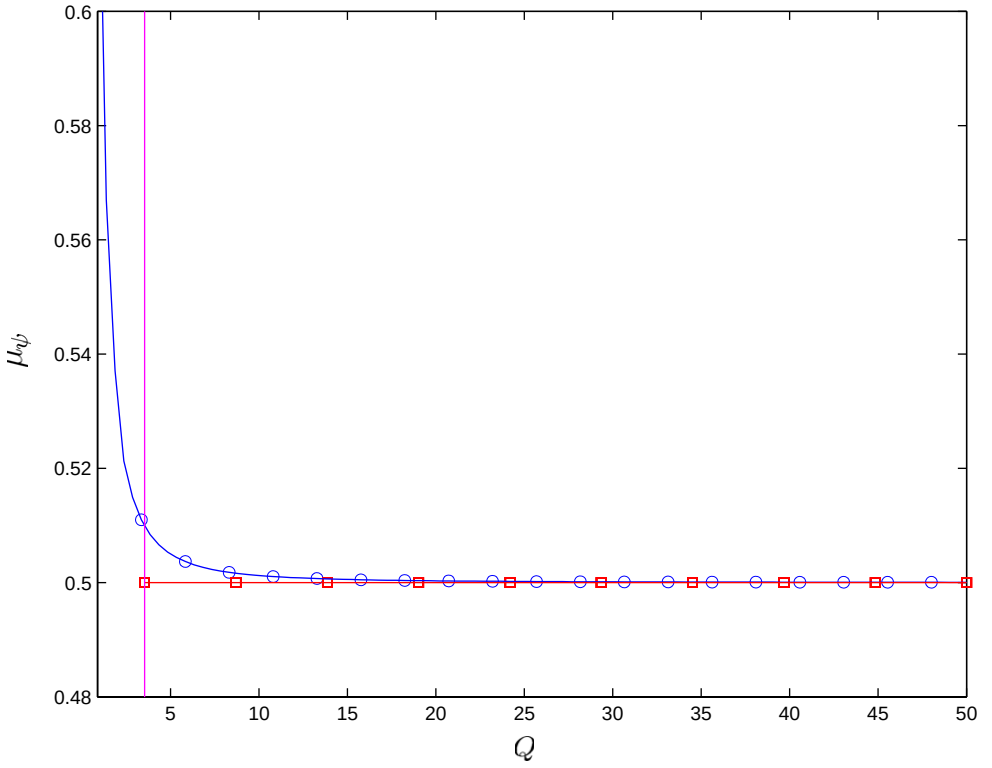


Fig. 2. Uncertainty $\mu_\psi$ of Cauchy wavelet ($\bigcirc$) and of Morlet wavelet ($\square$). Vertical line corresponding to $Q = \sqrt{5}/2$, numerically admissible limit of Morlet wavelet.

Let the two real coefficients $c_t$ and $c_f$ greater or equal to 1 be introduced such as when $t$ is outside the interval $I_{c_t} = [t_\psi - c_t\Delta t_\psi, t_\psi + c_t\Delta t_\psi]$ and when $\omega$ is outside the interval $I_{c_f} = [\omega_\psi - c_f\Delta\omega_\psi, \omega_\psi + c_f\Delta\omega_\psi]$, $\psi(t)$ and $\hat{\psi}(\omega)$ have good decreasing properties, respectively (this means that $\psi(t)$ and $\hat{\psi}(\omega)$ have null or very "small" values). It can be shown by the help of the Bienaymé–Tchebychev inequality, that when $t$ is outside $I_{c_t}$ and $\omega$ is outside $I_{c_f}$, then $\int_{\mathbb{R}-I_{c_t}} |\psi(t)|^2\,\mathrm{d}t \leqslant 1/c_t^2||\psi||_2^2$ and $\int_{\mathbb{R}-I_{c_f}} |\hat{\psi}(\omega)|^2\,\mathrm{d}\omega \leqslant 1/c_f^2||\hat{\psi}||_2^2$, respectively.

The effect of the values of $c_t$ and $c_f$ are then illustrated and three cases are considered: $c_t = c_f = 2$, $c_t = c_f = 5$ and $c_t = c_f = 8$. In Fig. 1, the vertical lines denote for both wavelets, the bounds of the intervals $I_{c_t}$ and $I_{c_f}$. It can be noted that the more $Q$ increases, the closer these lines become for the Morlet and Cauchy wavelets. More precisely, the ratios $r_\psi = |\psi(t_\psi + c_t\Delta t_\psi)|/|\psi(t_\psi)|$ and $r_{\hat{\psi}} = |\hat{\psi}(\omega_\psi + c_f\Delta\omega_\psi)|/|\hat{\psi}(\omega_\psi)|$ are proposed to characterize the properties of the decrease of $\psi(t)$ and $\hat{\psi}(\omega)$, respectively. In Ref. [26], it is shown that $r_\psi = r_\psi^* = \mathrm{e}^{-c_t^2/4}$ and $r_{\hat{\psi}} = r_{\hat{\psi}}^* = \mathrm{e}^{-c_f^2/4}$ for the Morlet wavelet. For the Cauchy wavelet, $r_\psi(Q)$ and $r_{\hat{\psi}}(Q)$ tend asymptotically when $Q$ tends to infinity, towards $r_\psi^*$ and $r_{\hat{\psi}}^*$, respectively. $r_\psi$ and $r_{\hat{\psi}}$ are drawn versus $Q$ in Fig. 3. The choice of $c_t = c_f = 5$ seems to be a good compromise.

Fig. 3. Extended localization of mother wavelet in time (a) and frequency (b) domains. — Cauchy wavelet, - - - Morlet wavelet corresponding to $\bigcirc : c_t = c_f = 2$, $\square : c_t = c_f = 5$ and $\triangle : c_t = c_f = 8$. Vertical line corresponding to $Q = \frac{\sqrt{5}}{2}$.

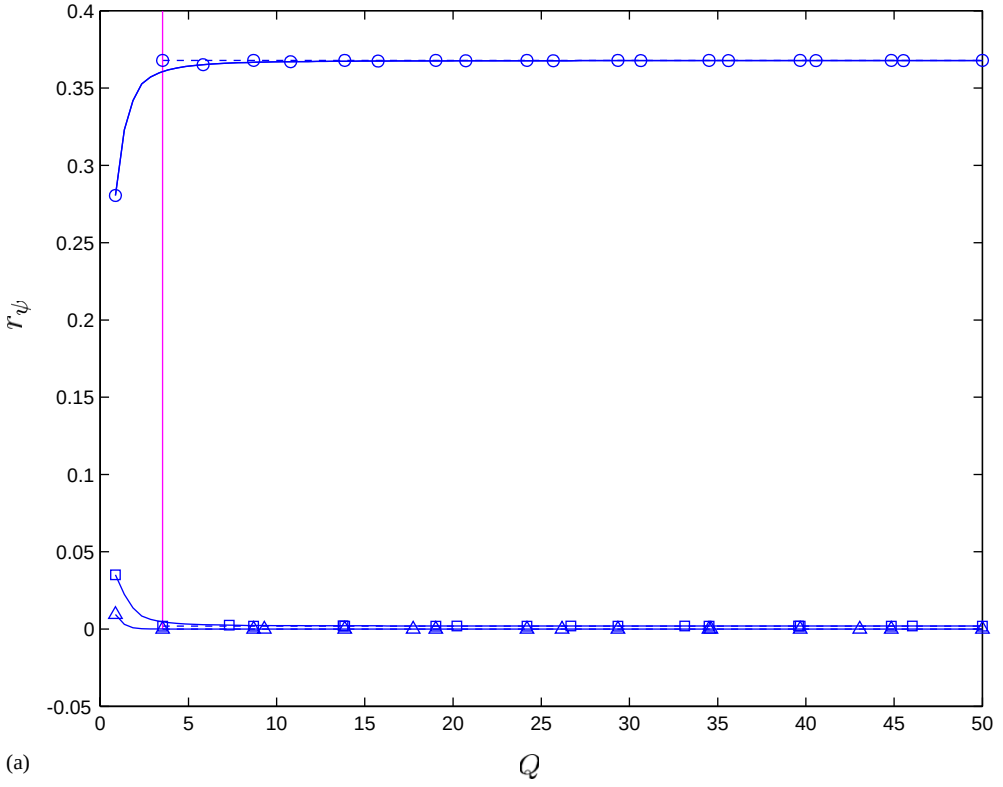
0.4
0.35
0.3
0.25
0.2
0.15
0.1
0.05
0
-0.05
$r_\psi$
0
5
10
15
20
25
30
35
40
45
50
$Q$

(a)

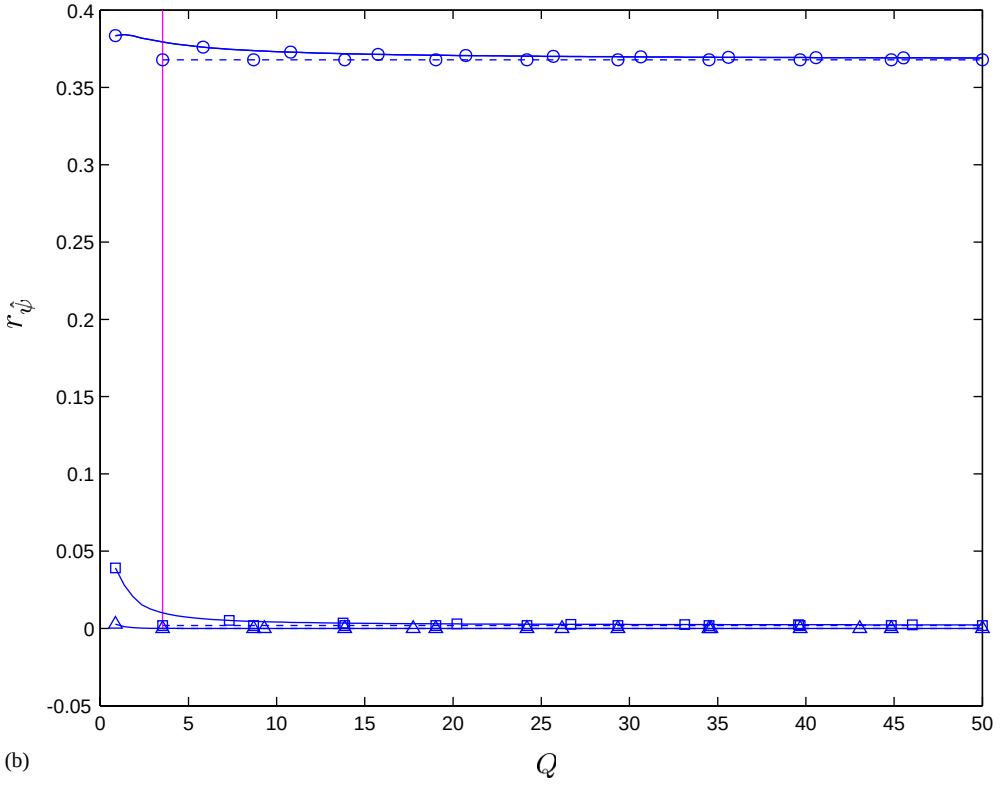
0.4
0.35
0.3
0.25
0.2
0.15
0.1
0.05
0
-0.05
$r_{\hat{\psi}}$
0
5
10
15
20
25
30
35
40
45
50
$Q$

(b)

Thus, it is proposed to define $D$ as an "extended" time–frequency localization domain for the CWT expressed in Eq. (9) around the phase point $(b_j, \omega_j = \omega_\psi/a_j)$. Using the coefficients $c_t$, $c_f$ and the progressive property of the mother wavelet, $D$ becomes

$$\left[b_j + \frac{\omega_\psi}{\omega_j} t_\psi - \frac{\omega_\psi}{\omega_j} c_t \Delta t_\psi, \quad b_j + \frac{\omega_\psi}{\omega_j} t_\psi + \frac{\omega_\psi}{\omega_j} c_t \Delta t_\psi\right] \times \left[\max\left(0, \omega_j\left(1 - c_f \frac{\Delta\omega_\psi}{\omega_\psi}\right)\right), \quad \omega_j\left(1 + c_f \frac{\Delta\omega_\psi}{\omega_\psi}\right)\right]. \tag{39}$$

$D$ must be included into $[0, L] \times [0, 2\pi f_{Nyquist}]$; this leads to the following system of inequalities:

$$\begin{cases} \dfrac{\omega_\psi}{\omega_j} c_t \Delta t_\psi - \dfrac{\omega_\psi}{\omega_j} t_\psi \leqslant b_j \leqslant L - \dfrac{\omega_\psi}{\omega_j} c_t \Delta t_\psi - \dfrac{\omega_\psi}{\omega_j} t_\psi \\ 0 < \omega_j \leqslant \dfrac{2\pi f_{Nyquist}}{1 + c_f(\Delta\omega_\psi/\omega_\psi)}. \end{cases} \tag{40}$$

Finally, by introducing $Q$ and $\mu_\psi$ and assuming $t_\psi = 0$, which is true for both Morlet and Cauchy wavelets, system (40) becomes

$$\frac{1}{\omega_j} c_t 2Q\mu_\psi \leqslant b_j \leqslant L - \frac{1}{\omega_j} c_t 2Q\mu_\psi, \tag{41}$$

$$0 < \omega_j \leqslant \frac{2\pi f_{Nyquist}}{1 + c_f(1/(2Q))}. \tag{42}$$

As shown by inequalities (41) and (42), $D$ is delimited by two hyperbolae whose equations are $\omega = (1/b)c_t 2Q\mu_\psi$ and $\omega = 1/(L - b)c_t 2Q\mu_\psi$ and two horizontal lines whose equations are $\omega = 0$ and $\omega = 2\pi f_{Nyquist}/(1 + c_f(1/2Q))$. Due to the introduction of the two parameters $c_t$ and $c_f$ greater than 1, the useful time interval is smaller than $L$ and the maximum useful frequency is smaller than $f_{Nyquist}$. This useful domain $D$ will be used for the modal identification procedure.

### 4.3. Mode decoupling—mother wavelet parameter choice

The next step is to be able to correctly extract two close ridges corresponding to two coupled modes. Note $\omega_j$ the angular eigenfrequency and $\mathrm{d}\omega_j$ the frequency discrepancy from which the effect of the modal coupling must be avoided. In order to solve this problem, the frequency localization domain of the CWT along a ridge, given in relation (39) $[\max(0, \omega_j(1 - c_f(\Delta\omega_\psi/\omega_\psi))), \omega_j(1 + c_f(\Delta\omega_\psi/\omega_\psi))]$ is assumed to be included into $[\omega_j - \mathrm{d}\omega_j, \omega_j + \mathrm{d}\omega_j]$. This leads to

$$Q \geqslant c_f \frac{\omega_j}{2\,\mathrm{d}\omega_j}. \tag{43}$$

It is proposed that $\mathrm{d}\omega_j = \min((\omega_j - \omega_{j-1}), (\omega_{j+1} - \omega_j))$ for $1 \leqslant j \leqslant N$ with $\omega_0 = 0$, $\omega_{N+1} = 2\pi f_{Nyquist}$. Thus, inequality (42) previously obtained is immediately checked since $\mathrm{d}\omega_j < \pi f_{Nyquist}$. Then relation (41) combined with the Heisenberg's inequality gives

$$Q \leqslant \frac{L\omega_j}{2c_t}, \tag{44}$$

and finally, the parameter $Q$ can be bounded by the following limits:

$$c_f \frac{\omega_j}{2\,\mathrm{d}\omega_j} \leqslant Q \leqslant \frac{L\omega_j}{2c_t}. \tag{45}$$

Here, $L$ and $f_{Nyquist}$ are obtained from measurements; $\omega_j$ can be evaluated by FFT and classified in increasing order. $c_t$ and $c_f$ must satisfy the following inequality:

$$c_t c_f \leqslant L\,\mathrm{d}\omega_j, \tag{46}$$

deduced from Eq. (45). It is proposed to start with $c_t = c_f = 5$. When inequality (46) is not checked, $c_t$ and $c_f$ must be reduced until (46) becomes true. Then, the value of $Q$ can be chosen in the limits fixed by Eq. (45). When the $Q$ value increases, the edge effect becomes more significant, thus the useful time interval for modal identification shrinks but the mode decoupling is more effective.

### 4.4. Full procedure for modal parameters identification of m.d.o.f systems

Using the properties of the CWT for processing frequency modulated signals, an identification procedure is proposed to obtain the values of modal parameters. The procedure is presented for displacement responses and can be easily extended to velocity or acceleration ones. It consists of three steps

(1) First step: compute the CWT of signal $u_k(t)$; the CWT of $\dot{u}_k(t)$ and of $\ddot{u}_k(t)$ can be deduced from Eq. (14). The choice of the mother wavelet and its parameters are based on the $Q$ value following relation (45). The choice of $Q$ depends on the spectral components in the signal as well as the sampling rate and the duration of the signals. The use of the peak picking technique applied to the FFT of the signal under study is enough to obtain some rough estimates of the modal frequencies in the signals and then allows the computation of the bounds of $Q$.

(2) Second step: estimate ridges and skeletons. The time variation of instantaneous frequencies $\dot{\alpha}^{measure}_{u_{kj}}(b)$ and of the analytical signals $Z^{measure}_{u_{kj}}(b)$ from the CWT of $u_k(t)$ can be deduced

$$\dot{\alpha}^{measure}_{u_{kj}}(b) = \frac{\dot{\phi}_\psi(0)}{a_{rkj}(b)}, \tag{47}$$

$$\begin{aligned} Z^{measure}_{u_{kj}}(b) &= \frac{2}{\hat{\psi}(a_{rkj}\dot{\alpha}^{measure}_{kj})}\, T_\psi[u^{measure}_{kj}](b, a_{rkj}(b)) \\ &\approx \frac{2}{\hat{\psi}\,(\dot{\phi}_\psi(0))} T_\psi[u^{measure}_{k}](b, a_{rkj}(b)). \end{aligned} \tag{48}$$

It is also possible to obtain $\dot{\alpha}^{measure}_{\dot{u}_{kj}}(b)$, $Z^{measure}_{\dot{u}_{kj}}(b)$, $\dot{\alpha}^{measure}_{\ddot{u}_{kj}}(b)$ and $Z^{measure}_{\ddot{u}_{kj}}(b)$ from ridges and skeletons of $T_\psi[\dot{u}^{measure}_k]$ and $T_\psi[\ddot{u}^{measure}_k]$ deduced in first step.

(3) Third step: identify modal parameters: $\tilde{\omega}_j$ (or $\omega_j$), $\xi_j$ and $\Phi_{kj}$. For each modal parameter, several adapted identification procedures are detailed with the expressions of $R^{measure}(b)$ and of $R^{model}(b)$ (see relations in Section 3.2):

(a) For *the angular frequency* $\tilde{\omega}_j$ (or $\omega_j$):
  (i) From ridge: $R^{measure}(b) = \dot{\alpha}^{measure}_{u_{kj}}(b)$ obtained from Eq. (47) and $R^{model}(b) = \tilde{\omega}_j$.
  (ii) From phase: $R^{measure}(b) = \angle Z^{measure}_{u_{kj}}(b)$ obtained from Eq. (48) and $R^{model}(b) = \tilde{\omega}_j t - \varphi_j + \frac{\pi}{2}(1 - \mathrm{sgn}(\Phi_{kj}))$.
  (iii) From modulus: $R^{measure}(b) = |Z^{measure}_{\dot{u}_{kj}}(b)|/|Z^{measure}_{u_{kj}}(b)|$ or $R^{measure}(b) = |Z^{measure}_{\ddot{u}_{kj}}(b)|/|Z^{measure}_{\dot{u}_{kj}}(b)|$ and $R^{model}(b) = \omega_j$.

(b) For *the damping ratio* $\xi_j$:
  (i) From modulus: $R^{measure}(b) = \log(|Z^{measure}_{u_{kj}}(b)|)$ and $R^{model}(b) = \log(A_{u_{kj}}) = \log(|\Phi_{kj}|\rho_j) - \xi_j\omega_j b$. The identified slope is an estimation of $-\xi_j\omega_j$. It is then easy to get $\xi_j$ and $\omega_j$ from the previous estimations of $-\xi_j\omega_j$ and $\tilde{\omega}_j$.
  (ii) From phase: $R^{measure}(b) = |\cos(\angle Z^{measure}_{u_{kj}}(b) - \angle Z^{measure}_{\dot{u}_{kj}}(b))|$ and $R^{model}(b) = \xi_j$.
  A similar procedure can be obtained by using $\ddot{u}$ instead of $\dot{u}$: $R^{measure}(b) = |\cos\left(\frac{\angle Z^{measure}_{\ddot{u}_{kj}}(b) - \angle Z^{measure}_{u_{kj}}(b)}{2}\right)|$ and $R^{model}(b) = \xi_j$.

(c) For *the mode shape* $\Phi_j$, The index $m$ is found by: $\max_k \sum_b |Z^{measure}_{u_{kj}}(b)|$.
  (i) absolute component $|\Phi_{kj}|$: $R^{measure}(b) = |Z^{measure}_{u_{kj}}(b)|/|Z^{measure}_{u_{mj}}(b)|$ and $R^{model}(b) = |\Phi_{kj}|/|\Phi_{mj}| = |\Phi_{kj}|$.
  (ii) the sign of $\Phi_{kj}$: $R^{measure}(b) = \angle Z^{measure}_{u_{kj}}(b) - \angle Z^{measure}_{u_{mj}}(b)$ and $R^{model}(b) = d^{km}_j(b) = \pi/2(1 - \mathrm{sgn}(\Phi_{kj}))$. Finally, $\Phi_{kj} = |\Phi_{kj}|\mathrm{sgn}(\Phi_{kj})$. It is noted that all above proposed identification methods are linear and lead to a direct estimation without iteration and initial conditions. Furthermore, the phase difference $d^{kl}_j(b) = \angle Z^{measure}_{u_{kj}}(b) - \angle Z^{measure}_{u_{lj}}(b)$ given in relation (33) characterizes the dissipation effect between two points $k$ and $l$ of the structure and thus can be used to detect the presence of non-proportional damping and/or non-linearity [18].

## 5. Application to simulated data

### 5.1. Illustration of edge effect and of different identification techniques

In order to illustrate the influence of the edge effect and the $Q$ parameter on the identification results, the procedure described in Section 4.4 is then applied to the free response of a s.d.o.f system whose mass $m = 1$ kg, rigidity $k = 7$ kN/m, damping coefficient $c = 2$ N s/m; initial conditions: $u(0) = 1$ m and $\dot{u}(0) = 0$ m/s; $L = 5$ s and $T = 0.0049$ s. Using $c_t = c_f = 5$ and $\mathrm{d}\omega_j = \omega_j - 0 = 83.6660$ rad/s, relation (45) gives the bounds of $Q$: $2.500 \leqslant Q \leqslant 41.833$. $T_\psi[u](b,a)$ is first computed from the displacement $u(t)$. $T_\psi[\dot{u}](b,a)$ and $T_\psi[\ddot{u}](b,a)$ are then deduced from Eq. (14). Fig. 4 shows the FT, CWT, relative errors between exact frequency (response modulus) of the response signal, and the estimated instantaneous frequency (response modules) based on CWT of the Cauchy wavelet with 1/3 octave filter ($Q = 4.3185$). All the modal parameter identification techniques presented in the full procedure 4.4 are tested with this $Q$ value. Figs. 5 and 6 present different functions $R^{measure}(t)$ for angular frequency and for damping ratio identifications respectively. The edge effect is delimited by two hyperbolae in the time–frequency plane illustrated in Fig. 4 and by vertical lines in the representation of functions $R^{measure}(t)$ of Figs. 5 and 6. The identified values are very similar and very close to the exact values for all the techniques, and identification errors are negligible inside the domain $D$ [26]. For practical reasons, the first

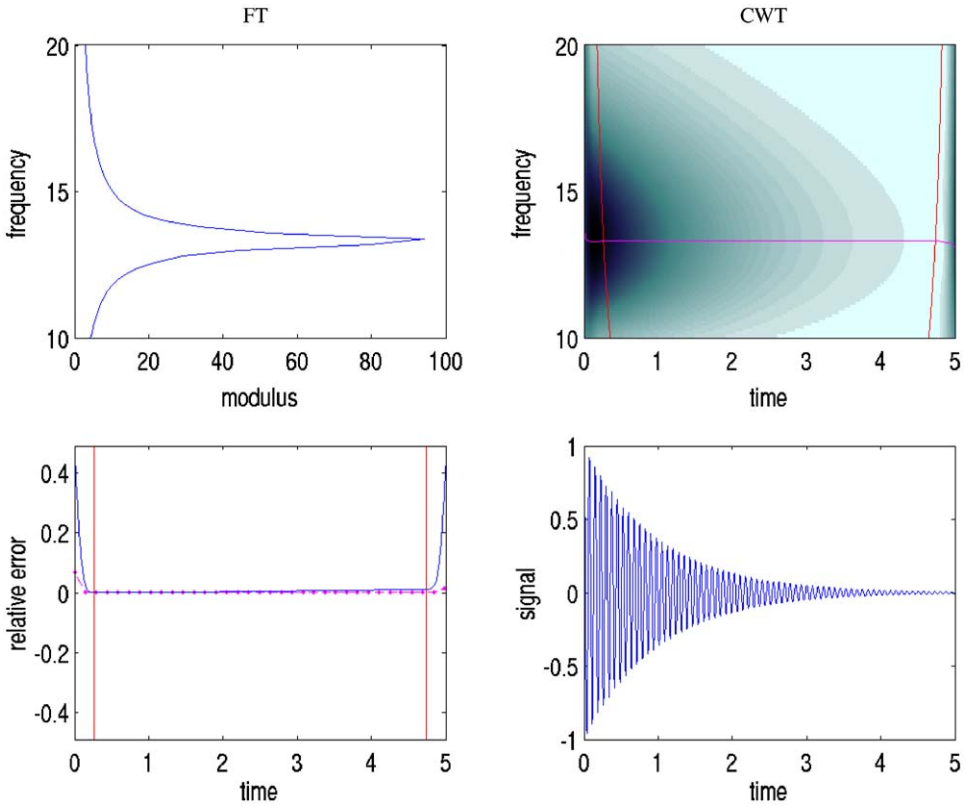


Fig. 4. Modulus of FT and of CWT using Cauchy wavelet 1/3 Octave of s.d.o.f system response. Relative errors of extracted ridge (frequency: – – –) and of associated analytical signal (modulus: —). Two hyperbolic curves and two vertical lines delimit edge effects on time–frequency plane and on extracted ridge respectively.

identification methods for angular frequency (i.e., from ridge) and damping ratio (i.e., from the slope of the logarithm of the modulus) can be selected. The identified modal parameters of the above s.d.o.f system obtained with these first methods, with the Morlet and Cauchy wavelets, for different values of $Q$, are given in Table 3. The results obtained with harmonic wavelets are unsatisfactory and not presented here. When $Q$ is small ($Q = 1.4142$), the computation with the Morlet wavelet is not performed since it is neither admissible nor progressive. With the Cauchy wavelet, this value of $Q$ is outside the bounds of $Q$ with $c_t = c_f = 5$ and inside the interval of $Q$ when $c_t = c_f \approx 3$; and the result is a little worse than those for higher $Q$ values due to a worse time–frequency localization of the Cauchy mother wavelet. When $Q$ increases, the extracted results are quite similar for the Morlet and Cauchy wavelets, due to the convergence of $r_\psi$ and $r_{\hat{\psi}}$, to the same limit for the two mother wavelets.

### 5.2. Validity test

The identification procedure presented above in Section 4.4 is then applied to the mass spring–damper model with four degrees of freedom illustrated in Fig. 7. The free displacements

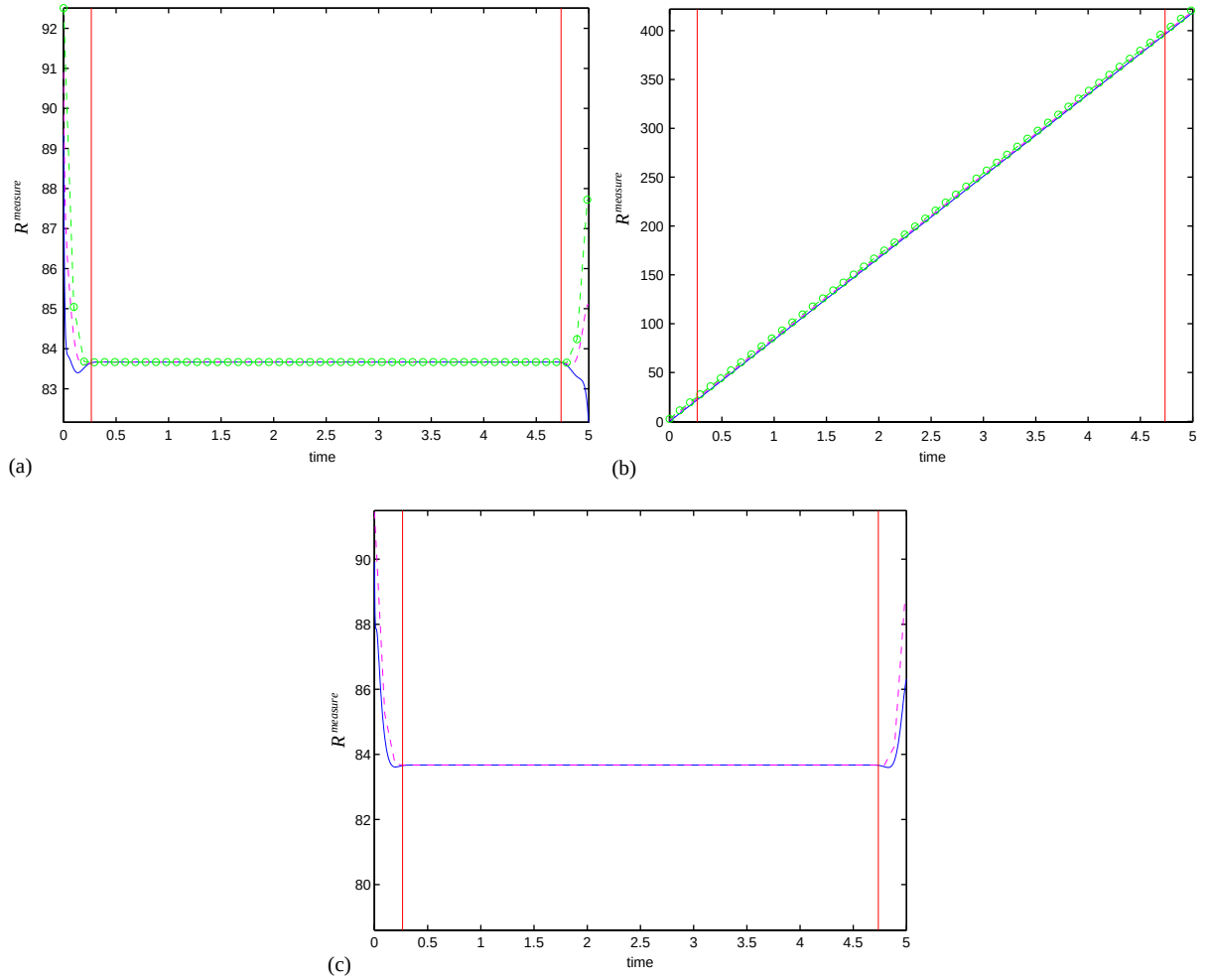


Fig. 5. Functions $R^{measure}(t)$ for angular frequency identification: (a) from ridge of: — displacement, - - - velocity and —○— acceleration; (b) from phase of: — displacement, - - - velocity and —○— acceleration; (c) from modulus ratios of:—velocity/displacement and - - - acceleration/velocity. Vertical lines delimit edge effects on the extracted ridge and skeleton.

$u_k(t), 1 \leqslant k \leqslant 4$ of the four masses of this model are plotted in Fig. 8 with initial conditions of displacements $[u_1(0) = 1.00, u_2(0) = 0.75, u_3(0) = 0.50, u_4(0) = 0.25]^{\mathrm{T}}(m)$ and of zero velocities. The sample of duration $L = 5$ s is taken over $M = 1024$ points (sampling period $T = 0.0049$ s). Analysis is performed for the $u_k(t)$ with both Cauchy and Morlet wavelets. The value $Q_j$ of $Q$ is chosen for each natural frequency $\omega_j$ following relation (45) with $c_t = c_f = 5$ and gathered in Table 4. The effect of the choice of $Q$ on the procedure is then illustrated with the Cauchy wavelet,

Fig. 6. Functions $R^{measure}(t)$ for damping ratio identification: (a) from modulus of: — displacement, - - - velocity and —○— acceleration; (b) from phase difference of: — displacement–velocity and —○— displacement–acceleration. Vertical lines delimit edge effects on the extracted ridge and skeleton.

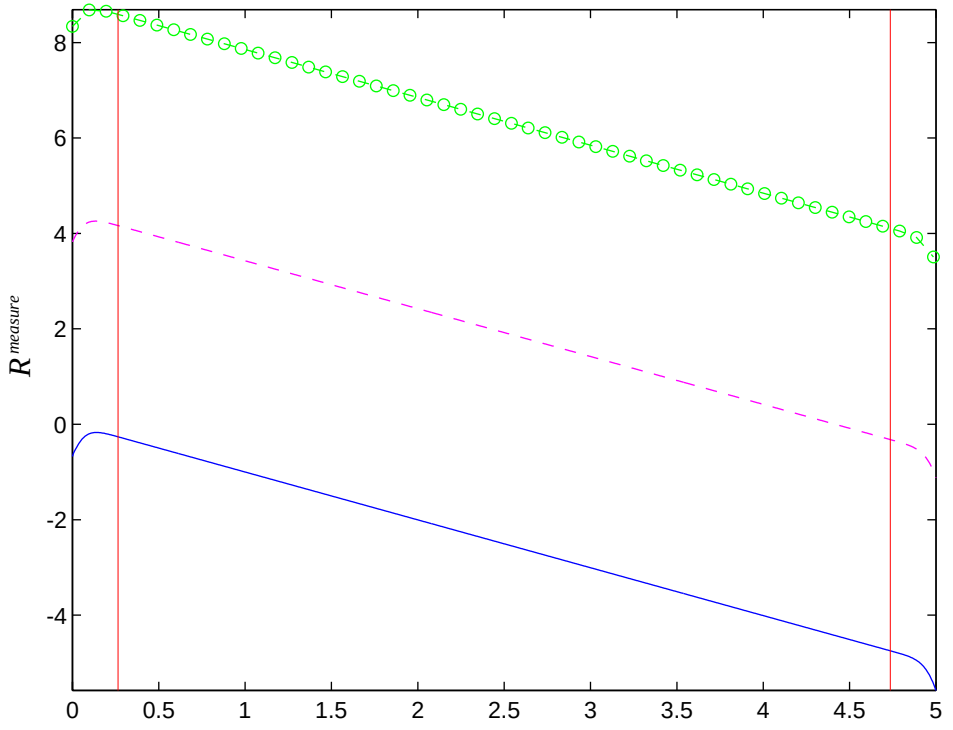
8
6
4
2
0
-2
-4
R measure
0
0.5
1
1.5
2
2.5
3
3.5
4
4.5
5
time

(a)

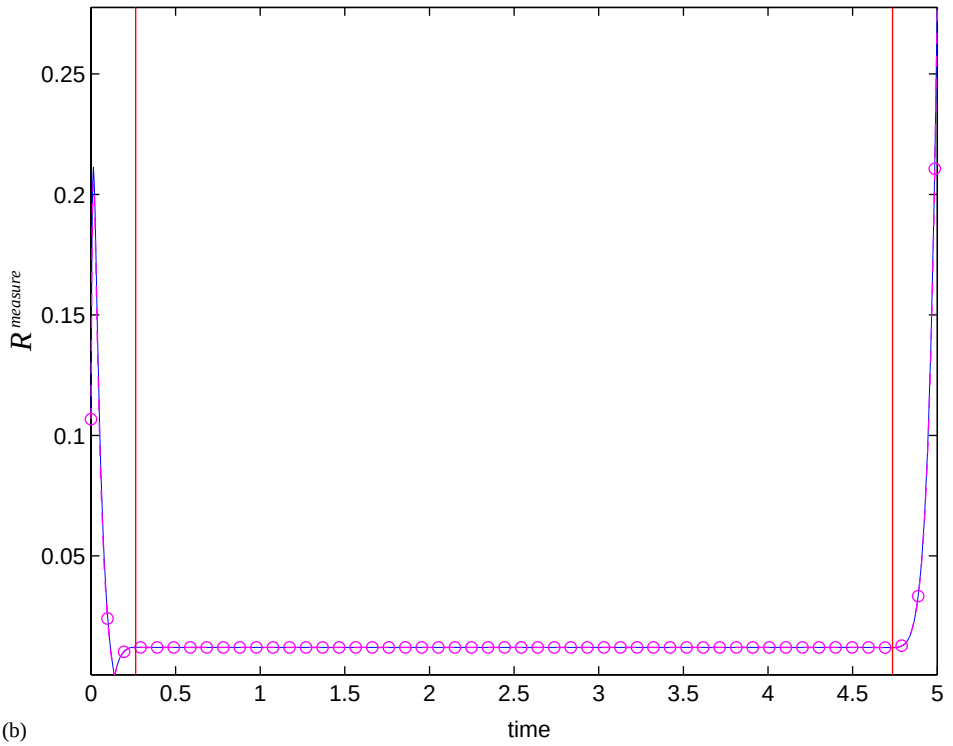
0.25
0.2
0.15
0.1
0.05
R measure
0
0.5
1
1.5
2
2.5
3
3.5
4
4.5
5
time

(b)

Table 3
Exact and identified modal parameters of the s.d.o.f system

| Filter | | Exact | | Morlet wavelet | | Cauchy wavelet | |
|---|---|---|---|---|---|---|---|
| Octave | Q | $\omega$ | $\xi$ | $\omega$ | $\xi$ | $\omega$ | $\xi$ |
| 1 | 1.4142 | 83.6660 | 0.0120 | — | — | 83.6749 | 0.0120 |
| 1/3 | 4.3185 | 83.6660 | 0.0120 | 83.6740 | 0.0120 | 83.6739 | 0.0120 |
| 1/6 | 8.6514 | 83.6660 | 0.0120 | 83.6740 | 0.0120 | 83.6739 | 0.0120 |
| 1/12 | 17.3099 | 83.6660 | 0.0120 | 83.6740 | 0.0120 | 83.6739 | 0.0120 |

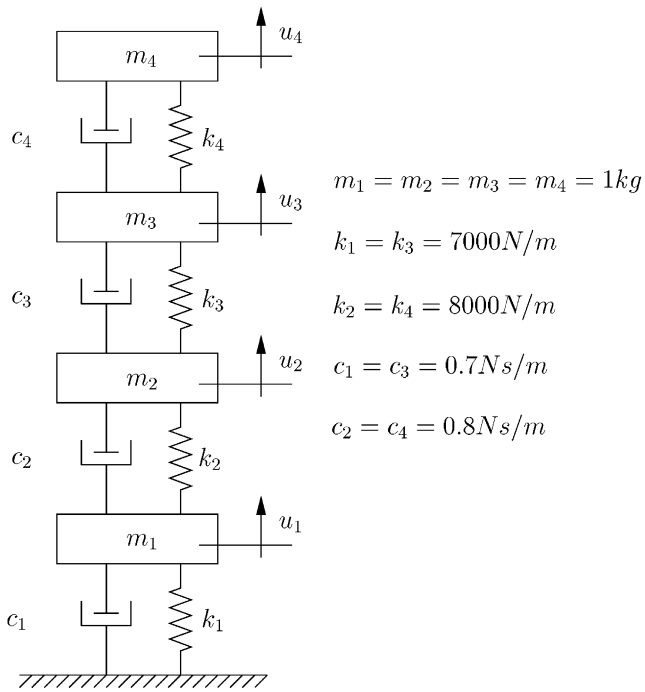


Fig. 7. Definition of the test 4-d.o.f system.

on this example. Figs. 9(a) and (b) show the signal $u_4(t)$, its FT and the logarithm of the modulus of the CWT computed with the Cauchy wavelet, for the values $Q_j$ previously obtained. In Fig. 9(a), $Q = Q_1 = 8$, the first mode can be easily distinguished but the third and fourth ones are coupled since the condition for mode decoupling is not checked: $10.5 \leqslant Q \leqslant 65.9$. $Q = Q_2 = 20$ is used for the extraction of the second mode but the first mode is now outside the useful domain $D$ previously defined. In Fig. 9(b), CWT is performed with $Q = Q_3 = Q_4 = 30$, the third and fourth modes are well separated: however, the useful time interval for the second mode is very short and the first mode is also outside of $D$. The identification procedure is then applied with the ridges and skeletons within $D$. Fig. 10 presents the first mode extracted as an example with the ridge (for identification of frequency), logarithm of modulus (for identification of damping ratio), ratios of

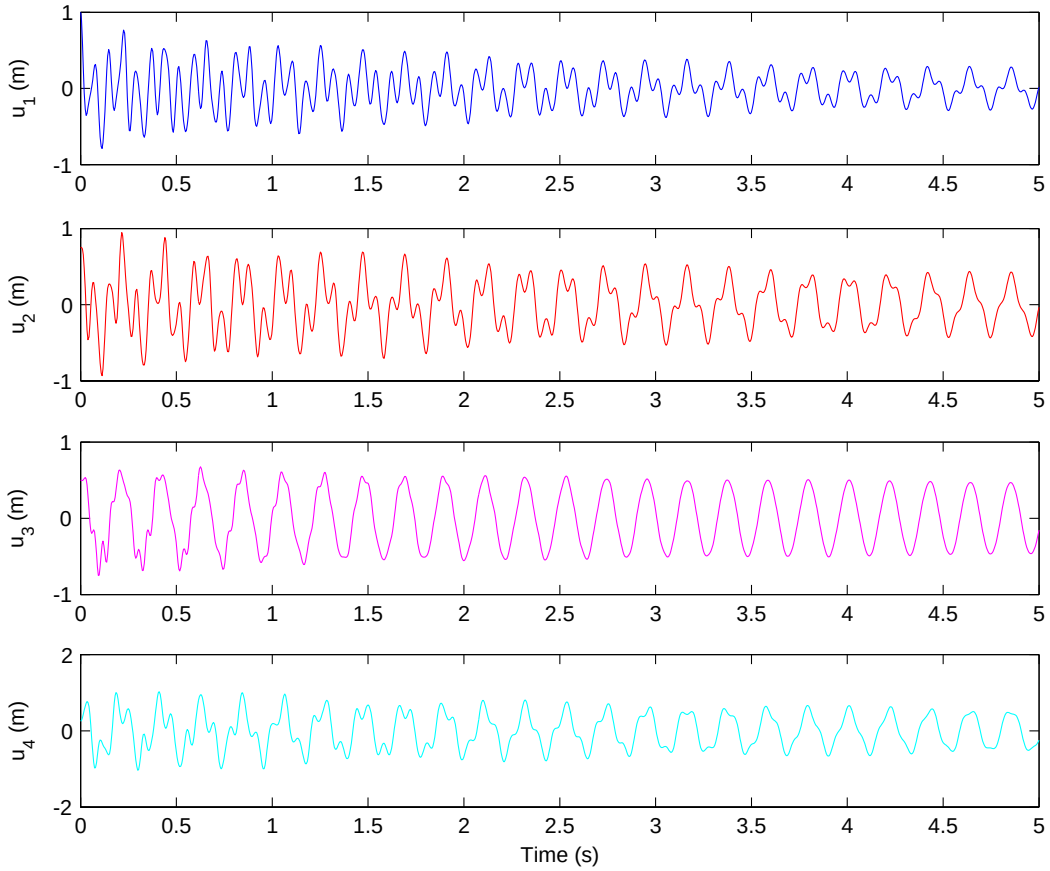


Fig. 8. Free responses of the test 4-d.o.f system ($u_k$ denotes the displacement of mass $m_k$).

Table 4
$Q$ values choice for CWT of the m.d.o.f test system

| $\omega_j$ | $d\omega_j$ | $c_f \frac{\omega_j}{2\,\mathrm{d}\omega_j} \leqslant Q \leqslant \frac{L\omega_j}{2c_t}$ | $Q_{chosen}$ |
|---|---|---|---|
| $10\pi$ | $10\pi$ | $2.500 \leqslant Q \leqslant 15.708$ | 8 |
| $27\pi$ | $17\pi$ | $3.971 \leqslant Q \leqslant 42.412$ | 20 |
| $42\pi$ | $10\pi$ | $10.500 \leqslant Q \leqslant 65.973$ | 30 |
| $52\pi$ | $10\pi$ | $13.000 \leqslant Q \leqslant 81.681$ | 30 |

modulus (for identification of absolute components of mode) and phase differences (for sign of components of mode). The identified modal parameters given in Table 5 and the mode shapes drawn in Fig. 11 obtained with Morlet and Cauchy mother wavelets are very close since $\mu_\psi(Q_j)$, $r_\psi(Q_j)$ and $r_{\hat{\psi}}(Q_j)$ are very similar for the two wavelets. It can be noted that estimated modal parameters and mode shapes match closely the exact values but not as well for the identified

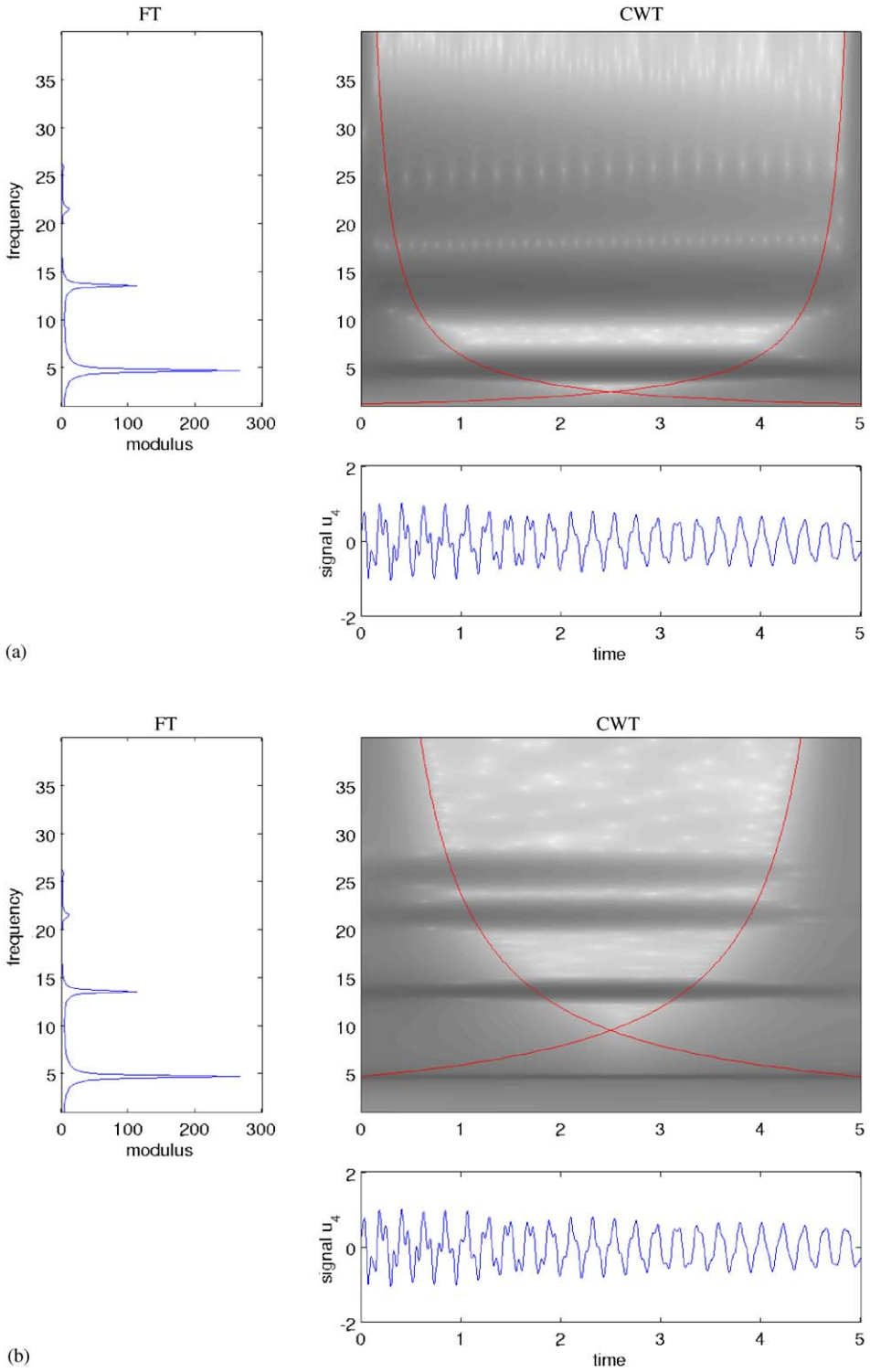


Fig. 9. Modulus of FT and logarithm of modulus of CWT of signal $u_4(t)$ using the Cauchy wavelet: (a) $Q = 8$ and (b) $Q = 30$. Hyperbolic curves delimit edge effects.

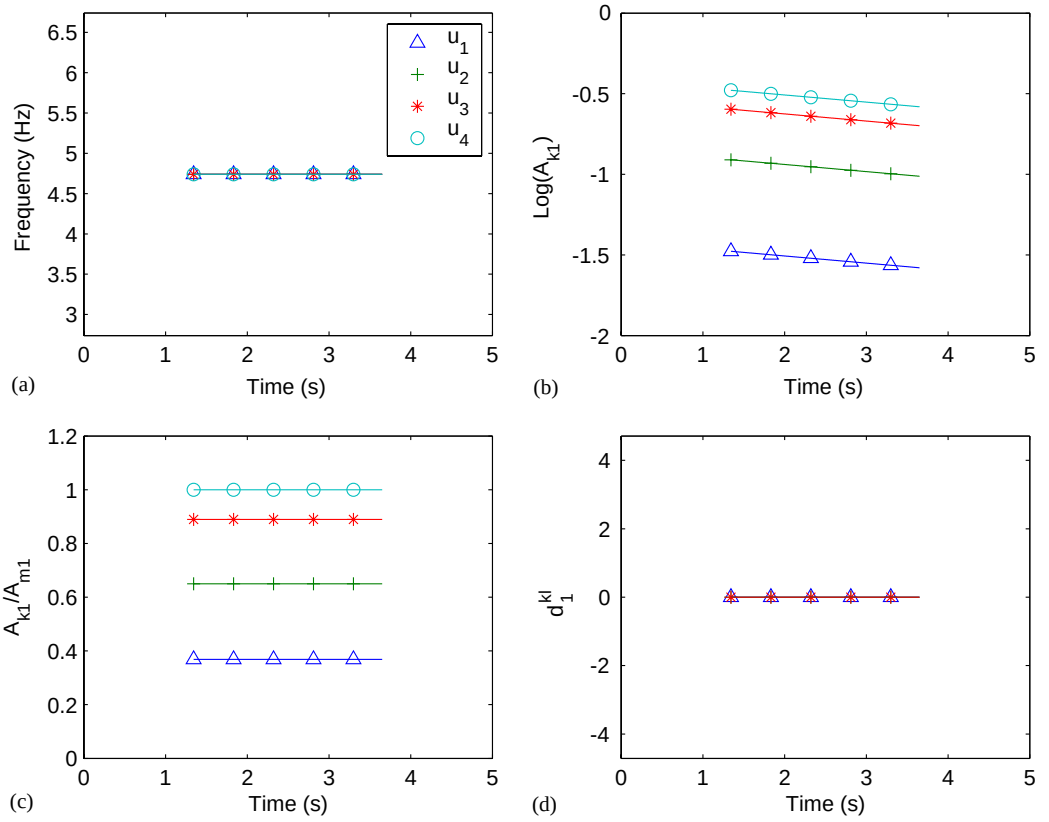


Fig. 10. Extracted instantaneous parameters of 1st mode from CWT using Cauchy wavelet, $Q = 8$ after removing edge effect. In subplots (a), (b) and (c), sensor 1: —△—, sensor 2: —+—, sensor 3: —∗—, sensor 4: —○—; in subplot (d), $d_1^{21}$: —Δ—, $d_1^{32}$: —+—, $d_1^{43}$: —∗—.

damping ratio of the fourth mode. The results agree well with the exact values, confirming the choice of the $c_t$, $c_f$ and $Q$ values.

## 6. Remarks and conclusions

This article concerns the modal identification from the free responses of m.d.o.f systems based on continuous wavelet transform. After a discussion of complex-valued mother wavelets, a complete modal identification procedure is established with improvements for numerical implementation. The parameter $Q$ is chosen to compare different mother wavelets and to characterize the quality of the CWT. Two interesting mother wavelets for identification procedure are retained and studied: Morlet and Cauchy. A thorough analysis demonstrated that the two mother wavelets behave asymptotically when $Q$ tends toward infinity. The modal parameters (frequencies, modal damping ratios and mode shapes) can be extracted from different methods and are tested on both s.d.o.f and m.d.o.f systems. The procedure is shown to be efficient with a

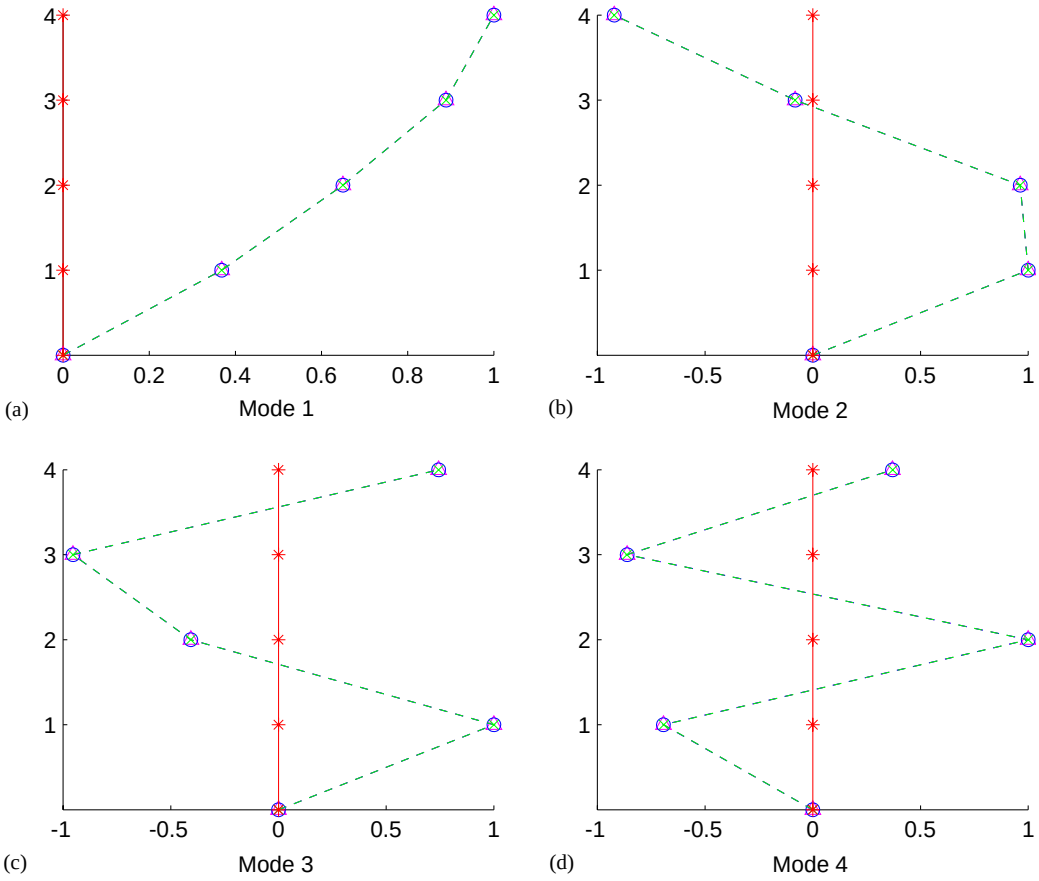


Fig. 11. Mode shapes of the test 4-DOF system.

Table 5
Exact and identified modal parameters of the m.d.o.f test system

| Mode | Exact frequency | Identified frequency (Hz) | | Exact damping ratio | Identified damping ratio (%) | |
|---|---|---|---|---|---|---|
| | (Hz) | Morlet | Cauchy | (%) | Morlet | Cauchy |
| 1 | 4.7397 | 4.7397 | 4.7396 | 0.15 | 0.15 | 0.15 |
| 2 | 13.5900 | 13.5905 | 13.5906 | 0.43 | 0.43 | 0.43 |
| 3 | 21.5035 | 21.5146 | 21.5145 | 0.68 | 0.67 | 0.67 |
| 4 | 25.9414 | 25.9764 | 25.9797 | 0.81 | 0.75 | 0.75 |

suitable choice of mother wavelet and their corresponding definition parameters. The edge effect is highlighted and the introduction of two real coefficients $c_t$ and $c_f$ allows this effect to be taken into account during the identification process. Moreover, some upper and lower bounds are given for $Q$ to facilitate the identification of coupled modes and to remedy the edge effect problem. The

efficiency of the improved technique with $c_t = c_f = 5$ and with different values of $Q$, depending to the mode under study, is tested in the case of a discrete system with four degrees of freedom. The identified modal parameters obtained with both wavelets are quite similar. The use of the Cauchy wavelet is legitimate when $Q$ is small ($Q \leqslant 5/\sqrt{2}$). When $Q$ increases, the results obtained with both wavelets become closer, a little better with the Morlet wavelet due to its excellent time–frequency localization. The facilities for processing either accelerations, velocities or displacements make the use of the Cauchy wavelet interesting for modal identification purposes. Finally, the proposed procedure can be easily extended to other linear time–frequency representations, such as the short time Fourier transform. The non-proportional damping and the identification of nonlinearities are also under study; preliminary results can be found in references [18,26].

## Acknowledgements

The authors would like to thank Prof. Nelly Point for stimulating discussions, and Ali Alshaer, Matthew Bussmann and Mark Collinson for their assistance in re-reading the English of the manuscript.

## References

[1] R.J. Allemang, D.L. Brown, A unified matrix polynomial approach to modal identification, *Journal of Sound and Vibration* 211 (3) (1998) 301–322.
[2] N.M.M. Maia, J.M.M. Silva, N. He, N.A. Jlieven, R.M. Lin, G.W. Skingle, W-M. To, A.P.V. Urgueira, *Theoretical and Experimental Modal Analysis*, Research Studies Press Ltd., Hertfordshire, 1998.
[3] D.L. Brown, R.J. Allemang, R. D. Zimmerman, M. Mergeay, Parameter estimation techniques for modal analysis, *SAE Paper Number 790221, SAE Transactions* 88 (1979) 828–846.
[4] S.R. Ibrahim, E.C. Mikulcik, A method for the direct identification of vibration parameters from the free responses, *Shock and Vibration Bulletin* 47 (4) (1977) 183–198.
[5] M.H. Richardson, Global frequency and damping estimates from frequency response measurements, in: *Proceedings of the Fourth International Modal Analysis Conference* (IMAC IV) Los Angeles, CA, 1986, pp. 465–470.
[6] M.H. Richardson, D.L. Formenti, Parameter estimation from frequency response measurements using rational fraction polynomials, in: *Proceedings of the First International Modal Analysis Conference* (IMAC I) Orlando, FL, 1982, pp. 167–181.
[7] N. Delprat, B. Escudie, P. Guillemain, R.K. Ronland-martinet, Ph. Tchamichian, B. Torrésani, Asymptotic wavelet and Gabor analysis: extraction of instantaneous frequencies, *IEEE* 38 (1992) 644–664.
[8] R. Carmona, W.L. Hwang, B. Torrésani, Identification of chirps with continuous wavelet transform, in: A. Antoniadis, G. Oppenheim (Eds.), *Wavelets and Statistics, Lecture Notes in Statistics*, Vol. 103, Springer, New York, 1994, pp. 95–108.
[9] B. Torrésani, *Analyse Continue par Ondelettes*, InterÉditions / CNRS Éditions, Paris, 1995.
[10] R. Carmona, W.L. Hwang, B. Torrésani, Characterization of signals by the ridges of their wavelet transforms, *IEEE Transactions on Signal Processing* 45 (1997) 2586–2589.
[11] R. Carmona, W-L. Hwang, B. Torrésani, *Practical Time–Frequency Analysis*, Gabor and Wavelet Transforms with an Implementation in S, Wavelet Analysis and its Applications, Vol. 9, Academic Press, San Diego, CA, 1998.
[12] B. Torrésani, Time–frequency and time-scale analysis, in: J.S. Byrnes (Ed.), *Signal Processing for Multimedia*, 1999, IOS Press, Amsterdam pp. 37–52.

[13] R. Carmona, W.L. Hwang, B. Torrésani, Multi-ridge detection and time–frequency reconstruction, *IEEE Transactions on Signal Processing* 47 (1999) 480–492.
[14] W.J. Staszewski, Identification of damping in m.d.o.f systems using time-scale decomposition, *Journal of Sound and Vibration* 203 (1997) 283–305.
[15] M. Ruzzene, A. Fasana, L. Garibaldi, B. Piombo, Natural frequencies and dampings identification using wavelet transform: application to real data, *Mechanical Systems and Signal Processing* 11 (1997) 207–218.
[16] P. Argoul, S. Hans, F. Conti, C. Boutin, Time–frequency analysis of free oscillations of mechanical structures. Application to the identification of the mechanical behavior of buildings under shocks, in: *Proceedings of the COST F3 Conference: System Identification and Structural Health Monitoring*, Madrid, Spain, 2000, pp. 283–292.
[17] P. Argoul, T-P. Le, Wavelet analysis of transient signals in civil engineering, in: M. Frémond, F. Maceri (Eds.), *Novel Approaches in Civil Engineering*, Lecture Notes in Applied and Computational Mechanics, Vol. 14, Springer, Berlin, 2003.
[18] P. Argoul, T-P. Le, Instantaneous indicators of structural behaviour based on continuous Cauchy wavelet transform, *Mechanical Systems and Signal Processing* 17 (2003) 243–250.
[19] D.E. Newland, Wavelet analysis of vibration, Part 1: Theory, *Journal of Vibration and Acoustics* 116 (1994) 409–416.
[20] D.E. Newland, Wavelet analysis of vibration, Part 2: Wavelet maps, *Journal of Vibration and Acoustics* 116 (1994) 417–425.
[21] D.E. Newland, Ridge and phase identification in the frequency analysis of transient signals by harmonic wavelets, *Journal of Vibration and Acoustics* 121 (1999) 149–155.
[22] S.K. Tang, On the time–frequency analysis of signals that decay exponentially with time, *Journal of Sound and Vibration* 234 (1999) 241–258.
[23] W.J. Staszewski, Identification of non-linear systems using multi-scale ridges and skeletons of the wavelet transform, *Journal of Sound and Vibration* 214 (1998) 639–658.
[24] C.K. Chui, in: Charles K. Chui (Ed.), *An Introduction to Wavelets*, Academic Press, San Diego, 1991.
[25] K. Gram-Hansen, K. Dorize, On the choice of parameters for time–frequency analysis, in: Y. Meyer (Ed.), *Wavelets and Applications*, *Proceedings of the International Conference*, Masson, Parts, 1991, pp. 86–92.
[26] T-P. Le, Auscultation Dynamique des Structures á l'Aide de l'Analyse continue en Ondelettes, Ph.D. Thesis, ENPC, 2003, (in French).
[27] M. Géradin, D. Rixen, *Théorie des Vibrations, Application à la Dynamique des Structures*, 2nd Edition, Masson, Paris, 1996.
[28] T. Paul, Ondelettes et Mécanique Quantique, Ph.D. Thesis, CPT Marseille, 1986 (in French).
[29] H-P. Yin, P. Argoul, Transformations intégrales et identification modale, *Comptes Rendus des Sciences de l'Academie des Sciences Paris. Série ii b* 327 (1999) 777–783.
[30] G-M. Zhang, C-G. Hou, Y-W. Wang, S-Y. Zhang, Optimal frequency-to-bandwidth ratio of wavelet in ultrasonic non-destructive evaluation, *Ultrasonics* 39 (2001) 13–17.
[31] J. Slavic, I. Simonovski, M. Boltezar, Damping identification using a continuous wavelet transform: application to real data, *Journal of Sound and Vibration* 262 (2003) 291–307.